Received: 8 December 2023 | Revised: 5 April 2024 | Accepted: 10 April 2024

DOI: 10.1002/nme.7538

RESEARCH ARTICLE

WILEY

A projection-based quaternion discretization of the geometrically exact beam model

Paul Wasmer | **Peter Betsch**

Institute of Mechanics, Karlsruhe Institute of Technology, Karlsruhe, Germany

Correspondence
Peter Betsch, Karlsruhe Institute of Technology, Otto-Amman-Platz 9, 76131 Karlsruhe, Germany.
Email: peter.betsch@kit.edu

Abstract

In the present work the geometrically exact beam model is formulated in terms of unit quaternions. A projection-based discretization approach is proposed which is based on a normalization of the quaternion approximation. The discretization relies on NURBS shape functions and, alternatively, on Lagrangian interpolation. The redundancy of the quaternions is resolved by applying the method of Lagrange multipliers. In a second step the Lagrange multipliers are eliminated circumventing the need to solve saddle point systems. The resulting finite elements retain the objectivity of the underlying beam formulation. Optimal rates of convergence are observed in representative numerical examples.

KEYWORDS

Bubnov–Galerkin method, finite rotations, isogeometric analysis, NURBS shape functions, quaternions, projection-based discretization

1 | INTRODUCTION

In many engineering applications it becomes necessary to simulate the behavior of slender structures. It is well-known in physics and engineering that slender structures can be approximated by beam models. One of the most important beam formulations suitable for the treatment of large deformations is the so-called geometrically exact beam model.[1–3] In the literature, it can also be found under many other names such as Simo–Reissner formulation, (special) Cosserat rod, or nonlinear Timoshenko beam. The geometrically exact beam model is described by quasi-linear partial differential equations, making a numerical solution method necessary. To this end, the finite element method is commonly applied.

Instead of using continuum elements, beam finite elements can achieve a significant size-reduction of the algebraic system to be solved. However, the reduction from a three-dimensional continuum to a beam model comes at a cost. Instead of a linear (or flat) configuration manifold in the case of continua, it becomes necessary to deal with a nonlinear manifold.[2] This is due to the fact that the orientation of the cross-sectional areas of the beam is independently described from the placement of its centerline. Accordingly, rotations of the cross-sections need to be accounted for. Rotation tensors belong to the special orthogonal group $SO(3)$, which forms an embedded smooth nonlinear manifold.[4–6]

Thus, in the design of finite elements for beams it becomes necessary to discretize either the special orthogonal group $SO(3)$ or some parametrization of it. Multiple different parametrizations of $SO(3)$ exist, for example, different global rotational angle descriptions such as Euler or Tait angels. Even though they represent a set of minimal coordinates, all parametrizations with three global angles exhibit singularities.[7]

Another approach to handle the special orthogonal group was introduced in References 8–10. There, a moving frame consisting of three so-called directors is considered. The director formulation coincides with the direct use of rotation tensors belonging to $SO(3)$.[11–13] Thus, the corresponding director interpolation circumvents any parametrization of $SO(3)$. However, in this approach the orthonormality constraint on the director frame is typically relaxed to the nodal points which complies with the interpolatory nature of the Lagrange shape functions. However, this implies that the director interpolation is not consistent with the underlying configuration manifold outside the nodal points. Moreover, this discretization approach cannot be applied in the framework of isogeometric analysis, since NURBS-based shape functions are not interpolatory,[14] so that the imposition of the orthonormality constraint in the control points would make no sense in general.

A very interesting alternative for the parametrization of the rotation group are unit quaternions.[15,16] One major advantage of unit quaternions is that they do not exhibit any singularities while staying close to the number of minimal coordinates. Furthermore, in contrast to rotational angles no trigonometric functions, which are in general computationally expensive, need to be evaluated to represent rotations.[17] They are thus often employed in computer graphics.[15,17] Unit quaternions were already applied multiple times to describe rotations in the context of beams. In the early work,[18] the geometrically exact beam model has been formulated in terms of unit quaternions. By applying a normalization procedure the unit-length of the quaternions and thus the orthogonality of the rotation tensor is ensured. However, finite elements are not considered in Reference 18.

In the context of beam finite elements, the interpolation of quaternions along with a subsequent normalization is addressed in Reference 11. However, a detailed treatment of the resulting finite element formulation is lacking. The option of employing spherical linear interpolation (SLERP) is also addressed in Reference 11. While in Reference 11 the focus lies on the use of rotation matrices, a quaternion-based SLERP formulation is investigated in Reference 12.

The SLERP approach is well-known from computer graphics[15,16] and connects two points on the manifold by a geodesic. Sander[19] introduces the concept of geodesic finite elements and applies it to the geometrically exact beam model formulated in terms of quaternions. The resulting approximation of the rotation field is equivalent to the quaternion-based SLERP approach. In essence, the SLERP discretization of rotations in the geometrically exact beam model can be traced back to Reference 20. At that time, the main motivation behind the work[20] was to obtain objective and path-independent beam finite elements. Indeed, early finite element discretizations of the geometrically exact beam model[21,22] were based on the interpolation of incremental rotations, which again live in a linear space, but were shown to be path-dependent.[20] Similarly, the interpolation of total rotations[23,24] was shown to yield nonobjective finite element formulations.

Recently, the SLERP-type approach to the discretization of $SO(3)$[20] has been extended to the special Euclidean group $SE(3)$.[25,26] Although this approach leads to quite involved formulations, they come with the advantage of being free of locking.[25,26]

In Reference 17 quaternions are interpolated by using Lagrange shape functions. The unit-length constraint on the quaternions is weakly enforced by means of the Lagrange multiplier method. The algebraic nature of the quaternions is used to yield semi-discrete equations of polynomial nonlinearity, which in turn is exploited in the numerical solution approach.

Besides classical Bubnov–Galerkin finite element methods, collocation methods for the discretization of the geometrically exact beam model relying on unit quaternions are investigated in References 27 and 28. Moreover, an isogeometric collocation method is applied to the quaternion-based geometrically exact beam model in Reference 29.

Using quaternions in the interpolation of finite rotations offers the possibility of applying a normalization procedure to ensure the pointwise orthonormality of the director frame. This way, a consistent approximation of finite rotations can be achieved. As pointed out above, quaternion interpolation and subsequent normalization has already been addressed in Reference 11 and was further investigated in References 13 and 30. This approach falls into the broader class of projection-based finite elements dealt with in Reference 31. In particular, it is shown in Reference 31 that projection-based finite elements are closely related to geodesic finite elements and yield optimal order of convergence. In the case of Reissner-Mindlin shells a projection-based finite element approach was proposed in Reference 32 to maintain the unit-length of the director field throughout the shell finite elements.

In the present work we use unit quaternions to describe the geometrically exact beam model. Of course, this approach is not new and has been followed in a number of previous works, many of which have been mentioned above. However, to the best of our knowledge, the discretization by means of unit quaternions has not been investigated in the framework of the isogeometric analysis of geometrically exact beams. It is one of the main goals of the present work to fill this gap. In particular, we present an in-depth treatment of the projection-based quaternion discretization relying on both Non-Uniform Rational B-Splines (NURBS) and Lagrange shape functions.

To resolve the redundancy of the quaternions, we investigate two alternative options for the enforcement of the unit-length constraint on the discrete quaternion field. While both alternative procedures rely on the Lagrange multiplier method, we show that one procedure is particularly well-suited for the size-reduction of the resulting algebraic problem. The size-reduction is based on the elimination of the discrete Lagrange multipliers without affecting the approximation properties of the underlying space discretization. Moreover, the size-reduction circumvents the necessity to solve an algebraic system with saddle point structure. A similar size-reduction procedure has previously been applied in the context of the director interpolation[8] and can be extended to the realm of dynamics.[33]

The rest of this work is structured as follows. In Section 2, we give a brief summary of quaternions and introduce a specific matrix notation which will be used in the sequel. Section 3 covers the geometrically exact beam model formulated in terms of quaternions. The projection-based finite element discretization of the underlying beam theory is dealt with in Section 4. The results of representative numerical examples are presented in Section 5. An appendix contains additional details of the proposed method such as the formulation of beam intersections in Appendix D. Eventually, conclusions are drawn in Section 6.

2 | QUATERNIONS

This section provides a short summary of main properties pertaining to quaternions needed in the sequel. We refer to References 15,34,35 for more background information. Denoting the set of quaternions by $\mathbb{H}$, a quaternion $\mathbb{q} \in \mathbb{H}$ is given by

$$\mathbb{q} = (q_0, \mathbf{q}) \tag{1}$$

and consists of a scalar real part $q_0 \in \mathbb{R}$ and a vector part $\mathbf{q} \in \mathbb{R}^3$. The product of two quaternions is defined by

$$\mathbb{q} \circ \mathbb{p} = (q_0 p_0 - \mathbf{q} \cdot \mathbf{p}, q_0 \mathbf{p} + p_0 \mathbf{q} + \mathbf{q} \times \mathbf{p}), \tag{2}$$

where the dot on the right-hand side denotes the standard scalar product and the cross represents the cross product of two vectors in $\mathbb{R}^3$. Due to the presence of the cross product in the vector part of the resulting quaternion, the quaternion product does not commute. The conjugate of a quaternion $\mathbb{q} \in \mathbb{H}$ is defined by

$$\overline{\mathbb{q}} = (q_0, -\mathbf{q}). \tag{3}$$

Furthermore, the norm of a quaternion is defined as for vectors in $\mathbb{R}^4$ by

$$\|\mathbb{q}\| = \sqrt{\mathbb{q} \cdot \mathbb{q}} = \sqrt{q_0^2 + q_1^2 + q_2^2 + q_3^2}. \tag{4}$$

Note that the norm is also referred to as the length of the quaternion. With this the inverse of a quaternion $\mathbb{q}^{-1}$ can be computed via

$$\mathbb{q}^{-1} = \frac{1}{\|\mathbb{q}\|^2} \overline{\mathbb{q}} \tag{5}$$

so that

$$\mathbb{q} \circ \mathbb{q}^{-1} = (1, \mathbf{0}), \tag{6}$$

where $(1, \mathbf{0}) \in \mathbb{H}$ is the identity element.

2.1 | Unit quaternions

Quaternions of unit length are of special interest since they can be used to represent rotations. Imposing the unit-length constraint $\mathbb{q} \cdot \mathbb{q} = 1$, we obtain the set of unit quaternions

$$S^3 = \{\mathbb{q} \in \mathbb{H} \mid \mathbb{q} \cdot \mathbb{q} = 1\} \tag{7}$$

which coincides with the unit sphere S^3 in $\mathbb{R}^4$. Importantly, S^3 is closed under quaternion multiplication introduced in (2). The rotation of a vector $\mathbf{a} \in \mathbb{R}^3$ can be expressed in terms of a unit quaternion $\mathbb{q} \in S^3$ through

$$\mathbb{q} \circ (0, \mathbf{a}) \circ \overline{\mathbb{q}} = (0, \mathbf{a}'), \tag{8}$$

where $\mathbf{a}' \in \mathbb{R}^3$ is the rotated vector, which can also be written as $\mathbf{a}' = \mathbf{R}(\mathbb{q})\mathbf{a}$ in terms of a rotation tensor $\mathbf{R}(\mathbb{q}) \in SO(3)$, the special orthogonal group in $\mathbb{R}^3$. The expression for the rotation tensor $\mathbf{R} : S^3 \mapsto SO(3)$ follows from the left-hand side of (8) by making use of the quaternion multiplication (2). Accordingly,

$$\mathbf{R}(\mathbb{q}) = (q_0^2 - \mathbf{q} \cdot \mathbf{q})\mathbf{I} + 2\mathbf{q} \otimes \mathbf{q} + 2q_0\hat{\mathbf{q}}. \tag{9}$$

Here, $\otimes$ stands for the dyadic product and $\hat{\mathbf{q}}$ is a skew-symmetric tensor, which follows from the relationship $\mathbf{q} \times \mathbf{a} = \hat{\mathbf{q}}\mathbf{a}$ for any $\mathbf{a} \in \mathbb{R}^3$. Writing vector $\mathbf{q} \in \mathbb{R}^3$ with respect to canonical base vectors $\mathbf{e}_i \in \mathbb{R}^3$ ($i = 1, \dots, 3$) as $\mathbf{q} = q_i\mathbf{e}_i$, where the summation convention applies to repeated indices, the corresponding matrix representation of $\hat{\mathbf{q}}$ is given by

$$\hat{\mathbf{q}} = \begin{bmatrix} 0 & -q_3 & q_2 \\ q_3 & 0 & -q_1 \\ -q_2 & q_1 & 0 \end{bmatrix}. \tag{10}$$

It is worth noting that the quaternion representation of $SO(3)$ does not exhibit any singularities which is in contrast to alternative representations in terms of three parameters.[7] Nevertheless, the parametrization of $SO(3)$ using unit quaternions is not unique as it covers the rotational group twice. In particular, formula (9) yields the same rotation tensor for $\mathbb{q}$ and $-\mathbb{q}$.

2.2 | Matrix representations of quaternion multiplication

In what follows it proves convenient to write the quaternion product defined in (2) by using specific matrices. Accordingly, the product of two quaternions $\mathbb{q}, \mathbb{p} \in \mathbb{H}$

$$\mathbb{v} = \mathbb{q} \circ \mathbb{p} \tag{11}$$

can also be written as

$$\mathbb{v} = \mathbf{Q}_l(\mathbb{q})\mathbb{p} = \mathbf{Q}_r(\mathbb{p})\mathbb{q} \tag{12}$$

by using matrices $\mathbf{Q}_l(\mathbb{q}), \mathbf{Q}_r(\mathbb{q}) \in \mathbb{R}^{4\times4}$ given by

$$\mathbf{Q}_l(\mathbb{q}) = \begin{bmatrix} \mathbb{q} & \mathbf{G}(\mathbb{q})^\mathsf{T} \end{bmatrix} \qquad \mathbf{Q}_r(\mathbb{q}) = \begin{bmatrix} \mathbb{q} & \mathbf{E}(\mathbb{q})^\mathsf{T} \end{bmatrix}, \tag{13}$$

where the 3×4 matrices

$$\mathbf{G}(\mathbb{q}) = \begin{bmatrix} -\mathbf{q} & q_0\mathbf{I}_3 - \hat{\mathbf{q}} \end{bmatrix} \qquad \mathbf{E}(\mathbb{q}) = \begin{bmatrix} -\mathbf{q} & q_0\mathbf{I}_3 + \hat{\mathbf{q}} \end{bmatrix} \tag{14}$$

have been used. The rotation tensor (9) can now be written in the form

$$\mathbf{R}(\mathbb{q}) = \mathbf{E}(\mathbb{q})\mathbf{G}(\mathbb{q})^\mathsf{T} \tag{15}$$

for any $\mathbb{q} \in S^3$. Further useful algebraic relationships involving the matrices $\mathbf{E}(\mathbb{p})$ and $\mathbf{G}(\mathbb{p})$ for any $\mathbb{p} \in \mathbb{H}$ can be summarized as follows:

$$\begin{aligned}\mathbf{E}(\mathbb{p})\mathbb{p} &= \mathbf{G}(\mathbb{p})\mathbb{p} = \mathbf{0},\\ \mathbf{E}(\mathbb{p})\mathbf{E}(\mathbb{p})^\top &= \mathbf{G}(\mathbb{p})\mathbf{G}(\mathbb{p})^\top = \|\mathbb{p}\|^2\mathbf{I}_3,\\ \mathbf{E}(\mathbb{p})^\top\mathbf{E}(\mathbb{p}) &= \mathbf{G}(\mathbb{p})^\top\mathbf{G}(\mathbb{p}) = \|\mathbb{p}\|^2\mathbf{I}_4 - \mathbb{p}\otimes\mathbb{p}.\end{aligned} \tag{16}$$

Moreover, for $\mathbb{p}, \mathbb{u} \in \mathbb{H}$

$$\begin{aligned}\mathbf{E}(\mathbb{p})\mathbb{u} &= -\mathbf{E}(\mathbb{u})\mathbb{p},\\ \mathbf{G}(\mathbb{p})\mathbb{u} &= -\mathbf{G}(\mathbb{u})\mathbb{p},\\ \mathbf{E}(\mathbb{p})\mathbf{G}(\mathbb{u})^\top &= \mathbf{E}(\mathbb{u})\mathbf{G}(\mathbb{p})^\top.\end{aligned} \tag{17}$$

We further define the skew-symmetric matrix $\overset{+}{\mathbf{v}} \in \mathbb{R}^{4\times4}$ mapping any vector $\mathbf{v} : \mathbb{R}^3 \to \mathbb{R}^{4\times4}$ such that

$$\mathbf{E}(\mathbb{p})^\top\mathbf{v} = \overset{+}{\mathbf{v}}\mathbb{p} \qquad \text{where} \qquad \overset{+}{\mathbf{v}} = \begin{bmatrix} 0 & -\mathbf{v}^\top \\ \mathbf{v} & \hat{\mathbf{v}} \end{bmatrix} \tag{18}$$

for any $\mathbb{p} \in \mathbb{H}$ and $\mathbf{v} \in \mathbb{R}^3$.

3 | GEOMETRICALLY EXACT BEAM FORMULATION

3.1 | Configuration space of the beam

The beam formulation relies on the reference curve $\boldsymbol{\varphi} \in \mathbb{R}^3$ parametrized in terms of the arc-length $s \in [0, L]$, where L is the length of the beam in the reference configuration (Figure 1). To every point s on the reference curve there are attached two directors $\mathbf{d}_1(s), \mathbf{d}_2(s) \in \mathbb{R}^3$ which span the cross-sectional plane. The third director $\mathbf{d}_3(s) \in \mathbb{R}^3$ points into the normal direction of the cross-sectional plane. The three directors are assumed to be mutually orthonormal so that the director frame can be expressed in terms of a rotation tensor $\mathbf{R}(s) \in SO(3)$ via

$$\mathbf{d}_i(s) = \mathbf{R}(s)\mathbf{e}_i \tag{19}$$

for $i = 1, \dots, 3$, where the Cartesian base vectors $\mathbf{e}_i \in \mathbb{R}^3$ form an inertial reference frame. The configuration space of the geometrically exact beam model can be written as

$$\tilde{\mathbb{Q}} = \{(\boldsymbol{\varphi}, \mathbf{R}) : [0, L] \to \mathbb{R}^3 \times SO(3)\}. \tag{20}$$

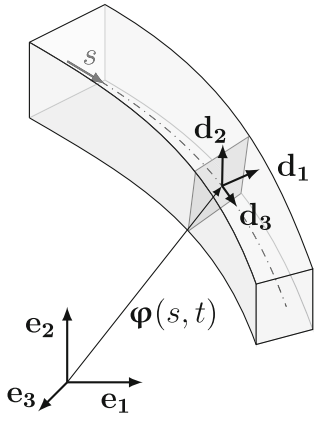

FIGURE 1 Sketch of a geometrically exact beam configuration.

In the present work we employ unit quaternions to represent the rotation tensor. Accordingly, instead of (19), the directors are expressed in terms of the unit quaternion $\mathbb{q}(s) \in S^3$ through the relationship

$$(0, \mathbf{d}_i(s)) = \mathbb{q}(s) \circ (0, \mathbf{e}_i) \circ \overline{\mathbb{q}}(s). \tag{21}$$

Alternatively, we may write $\mathbf{d}_i = \mathbf{R}(\mathbb{q})\mathbf{e}_i$, where the rotation tensor $\mathbf{R} : S^3 \mapsto SO(3)$ assumes the form (9). Correspondingly, the configuration space of the beam is now given by

$$\mathbb{Q} = \{(\boldsymbol{\varphi}, \mathbb{q}) : [0, L] \to \mathbb{R}^3 \times S^3\}. \tag{22}$$

Since $\mathbb{q} \in S^3$ implies the unit-length condition $\mathbb{q} \cdot \mathbb{q} = 1$, the derivative of this condition with respect to the arc-length yields $\mathbb{q}_{,s} \cdot \mathbb{q} = 0$, so that $\mathbb{q}_{,s} \in T_{\mathbb{q}}S^3$, the tangent space of S^3 at $\mathbb{q} \in S^3$ given by

$$T_{\mathbb{q}}S^3 = \{\mathbb{v} \in \mathbb{H} \mid \mathbb{q} \cdot \mathbb{v} = 0\}. \tag{23}$$

3.2 | Strain measures

In this section we provide the strain measures of the geometrically exact beam model based on the parametrization $(\boldsymbol{\varphi}, \mathbb{q}) \in \mathbb{Q}$. We start with the strains associated with bending and twist which can be arranged in vector $\mathbf{K} \in \mathbb{R}^3$. Vector $\mathbf{K}$ is defined as axial vector associated with the skew-symmetric tensor*

$$\widehat{\mathbf{K}} = \mathbf{R}^{\mathsf{T}}\mathbf{R}_{,s}. \tag{24}$$

Since

$$\mathbf{R}_{,s} = \left(\mathbf{E}(\mathbb{q})\mathbf{G}(\mathbb{q})^{\mathsf{T}}\right)_{,s} = 2\mathbf{E}(\mathbb{q})\mathbf{G}(\mathbb{q}_{,s})^{\mathsf{T}} \tag{25}$$

(24) yields

$$\widehat{\mathbf{K}} = 2\mathbf{G}(\mathbb{q})\mathbf{G}(\mathbb{q}_{,s})^{\mathsf{T}}, \tag{26}$$

where $(17)_3$ and $(16)_1$ have been used. It can be shown that the axial vector corresponding to (26) is given by

$$\boxed{\mathbf{K} = 2\mathbf{G}(\mathbb{q})\mathbb{q}_{,s}.} \tag{27}$$

For completeness this is shown in Appendix A. Note that strain measure (27) can also be written as

$$(0, \mathbf{K}) = 2\mathbf{Q}_l(\mathbb{q})^{\mathsf{T}}\mathbb{q}_{,s} = 2\overline{\mathbb{q}} \circ \mathbb{q}_{,s}. \tag{28}$$

The second strain measure of the geometrically exact beam model is defined by $\boldsymbol{\Gamma} = \mathbf{R}^{\mathsf{T}}\boldsymbol{\varphi}_{,s} - \mathbf{e}_3$ and accounts for transverse shear and normal strain. The representation of the rotation group by means of unit quaternions leads to

$$\boxed{\boldsymbol{\Gamma} = \mathbf{R}(\mathbb{q})^{\mathsf{T}}\boldsymbol{\varphi}_{,s} - \mathbf{e}_3,} \tag{29}$$

where the rotation tensor has been introduced in (15)

$$(0, \boldsymbol{\Gamma}) = \overline{\mathbb{q}} \circ (0, \boldsymbol{\varphi}_{,s}) \circ \mathbb{q} - (0, \mathbf{e}_3). \tag{30}$$

3.2.1 | Frame-indifference of the strain measures

The strain measures of the beam theory at hand are invariant under rigid motions. The so-called frame-indifference (or objectivity) of the strains can be shown by considering a superposed rigid motion of the beam defined by

$$\begin{aligned}(0,\boldsymbol{\varphi}^{\#}) &= \mathbb{r}\circ(0,\boldsymbol{\varphi})\circ\overline{\mathbb{r}} + (0,\mathbf{c}),\\ \mathbb{q}^{\#} &= \mathbb{r}\circ\mathbb{q}.\end{aligned} \tag{31}$$

Here, $\mathbb{r} \in S^3$ represents an arbitrary rotation while $\mathbf{c} \in \mathbb{R}^3$ represents an arbitrary translation. Inserting $(31)_1$ into (28) yields

$$\begin{aligned}(0,\mathbf{K}^{\#}) &= 2\overline{\mathbb{q}}^{\#}\circ\mathbb{q}^{\#}_{,s}\\ &= 2\overline{\mathbb{q}}\circ\overline{\mathbb{r}}\circ\mathbb{r}\circ\mathbb{q}_{,s}\\ &= 2\overline{\mathbb{q}}\circ\mathbb{q}_{,s}\\ &= (0,\mathbf{K})\end{aligned} \tag{32}$$

which shows the invariance of $\mathbf{K}$ under rigid motions. Similarly, substituting from (31) into (30) yields

$$\begin{aligned}(0,\boldsymbol{\Gamma}^{\#}) &= \overline{\mathbb{q}}^{\#}\circ(0,\boldsymbol{\varphi}^{\#}_{,s})\circ\mathbb{q}^{\#} - (0,\mathbf{e}_3)\\ &= \overline{\mathbb{q}}\circ\overline{\mathbb{r}}\circ\mathbb{r}\circ(0,\boldsymbol{\varphi}_{,s})\circ\overline{\mathbb{r}}\circ\mathbb{r}\circ\mathbb{q} - (0,\mathbf{e}_3)\\ &= \overline{\mathbb{q}}\circ(0,\boldsymbol{\varphi}_{,s})\circ\mathbb{q} - (0,\mathbf{e}_3)\\ &= (0,\boldsymbol{\Gamma}).\end{aligned} \tag{33}$$

In the present work we aim at a beam finite element formulation that inherits the frame-indifference of the strain measures from the underlying continuous formulation, compare References 8 and 20.

3.3 | Weak form

The weak form of the equilibrium problem pertaining to the present beam formulation can be written in the standard form

$$G_{\text{int}}(\boldsymbol{\varphi},\mathbb{q};\delta\boldsymbol{\varphi},\delta\mathbb{q}) = G_{\text{ext}}(\boldsymbol{\varphi},\mathbb{q};\delta\boldsymbol{\varphi},\delta\mathbb{q}) \tag{34}$$

for $(\boldsymbol{\varphi},\mathbb{q}) \in \mathbb{Q}$ and arbitrary admissible variations $(\delta\boldsymbol{\varphi},\delta\mathbb{q}) \in T_{(\boldsymbol{\varphi},\mathbb{q})}\mathbb{Q}$ lying in the tangent space

$$T_{(\boldsymbol{\varphi},\mathbb{q})}\mathbb{Q} = \{(\delta\boldsymbol{\varphi},\delta\mathbb{q}) : [0,L] \to \mathbb{R}^3 \times T_{\mathbb{q}}S^3\}. \tag{35}$$

The virtual work contribution of the internal forces results from

$$G_{\text{int}}(\boldsymbol{\varphi},\mathbb{q};\delta\boldsymbol{\varphi},\delta\mathbb{q}) = \int_0^L \delta\boldsymbol{\Gamma}\cdot\mathbf{N} + \delta\mathbf{K}\cdot\mathbf{M}\,\mathrm{d}s. \tag{36}$$

For the stress resultants $\mathbf{N}$ and $\mathbf{M}$ Saint–Vernant type constitutive laws of the form $\mathbf{N} = \mathbf{D}_1\boldsymbol{\Gamma}$ and $\mathbf{M} = \mathbf{D}_2\mathbf{K}$ are assumed. The stiffness tensors are given by $\mathbf{D}_1 = \text{diag}(GA, GA, EA)$ and $\mathbf{D}_2 = \text{diag}(EI_1, EI_2, GI_p)$, respectively. Starting from the strain measures (27) and (29), a straightforward calculation taking into account (17) yields

$$\begin{aligned}G_{\text{int}}(\boldsymbol{\varphi},\mathbb{q};\delta\boldsymbol{\varphi},\delta\mathbb{q}) = \int_0^L &\left(\delta\boldsymbol{\varphi}_{,s}\cdot\mathbf{E}(\mathbb{q}) + 2\boldsymbol{\varphi}_{,s}\cdot\mathbf{E}(\delta\mathbb{q})\right)\mathbf{G}(\mathbb{q})^{\top}\mathbf{N}\\ &+ 2\left(\delta\mathbb{q}_{,s}\cdot\mathbf{G}(\mathbb{q})^{\top} - \delta\mathbb{q}\cdot\mathbf{G}(\mathbb{q}_{,s})^{\top}\right)\mathbf{M}\mathrm{d}s.\end{aligned} \tag{37}$$

The virtual work contribution of the external loading is given by

$$G_{\text{ext}}(\boldsymbol{\varphi},\mathbb{q};\delta\boldsymbol{\varphi},\delta\mathbb{q}) = \int_0^L \delta\boldsymbol{\varphi}\cdot\overline{\mathbf{n}} + \delta\mathbf{q}\cdot 2\mathbf{E}(\mathbb{q})^{\top}\overline{\mathbf{m}}\,\mathrm{d}s, \tag{38}$$

where $\overline{\mathbf{n}} \in \mathbb{R}^3$ and $\overline{\mathbf{m}} \in \mathbb{R}^3$ are prescribed external forces and torques, respectively, acting along the centerline of the beam. Note that, for simplicity, boundary terms have been neglected in the above description.

4 | FINITE ELEMENT FORMULATION

We aim at a finite element formulation of the present beam model that both inherits the objectivity of the strain measures and preserves the unit-length of the quaternion field governing the rotation of the director frame throughout the discrete beam formulation. For that purpose the unit quaternion field is approximated by

$$\mathbb{q}^h(s) = \frac{\mathbb{p}^h(s)}{\|\mathbb{p}^h(s)\|}, \quad \text{where} \quad \mathbb{p}^h(s) = \sum_{i=1}^{n} N_i(s)\mathbb{p}_i. \tag{39}$$

As basis functions $N_i(s)$ we employ either NURBS shape functions (see Section 4.1 for further details) or standard Lagrange shape functions. Correspondingly, $\mathbb{p}_i \in \mathbb{H}$ are either the values at the control points or the nodal values of the discretized quaternions, respectively.

Note that the normalization of the discretized quaternion field (39) ensures that the discrete quaternions belong pointwise to the set of unit quaternions which are employed to parametrize the rotation manifold. That is, $\mathbb{q}^h \in S^3$ holds throughout the discrete beam formulation.

Taking the derivative of (39) with respect to the arc-length yields

$$\mathbb{q}^h_{,s} = \frac{\mathbb{p}^h_{,s}}{\|\mathbb{p}^h\|} - \mathbb{p}^h \frac{1}{\|\mathbb{p}^h\|^3}\left(\mathbb{p}^h \cdot \mathbb{p}^h_{,s}\right) = \frac{1}{\|\mathbb{p}^h\|}\mathbf{P}(\mathbb{q}^h)\mathbb{p}^h_{,s}, \tag{40}$$

where relation (4) has been taken into account. Moreover, $\mathbf{P}(\mathbb{q}^h)$ is a projector onto the tangent space of the unit sphere given by Reference 37

$$\mathbf{P}(\mathbb{q}^h) = \mathbf{I}_4 - \mathbb{q}^h \otimes \mathbb{q}^h. \tag{41}$$

Thus (40) ensures that $\mathbb{q}^h_{,s} \in T_{\mathbb{q}^h}S^3$. Similarly, variations of $\mathbb{q}^h \in S^3$ can be written in the form

$$\delta\mathbb{q}^h = \frac{1}{\|\mathbb{p}^h\|}\mathbf{P}(\mathbb{q}^h)\delta\mathbb{p}^h \tag{42}$$

ensuring that $\delta\mathbb{q}^h \in T_{\mathbb{q}^h}S^3$ for any

$$\delta\mathbb{p}^h(s) = \sum_{i=1}^{n} N_i(s)\delta\mathbb{p}_i. \tag{43}$$

Concerning the finite element approximation of the center line of the beam we apply the standard discretization

$$\boldsymbol{\varphi}^h(s) = \sum_{i=1}^{n} N_i(s)\boldsymbol{\varphi}_i \tag{44}$$

along with

$$\delta\boldsymbol{\varphi}^h(s) = \sum_{i=1}^{n} N_i(s)\delta\boldsymbol{\varphi}_i \tag{45}$$

for the corresponding test function. Again, $\boldsymbol{\varphi}_i, \delta\boldsymbol{\varphi}_i \in \mathbb{R}^3$ play the role of either the respective values at the control points, or the nodal values. In the sequel, we shall refer to the ith point of the discretization as control/nodal point.

We emphasize that the present discretization approach respects the configuration space of the geometrically exact beam model in the sense that $(\boldsymbol{\varphi}^h, \mathbb{q}^h) \in \mathbb{Q}$ and $(\delta\boldsymbol{\varphi}^h, \delta\mathbb{q}^h) \in T_{(\boldsymbol{\varphi}^h, \mathbb{q}^h)}\mathbb{Q}$, respectively.

4.1 | NURBS shape functions

As mentioned above, in addition to standard Lagrange shape functions we make use of NURBS shape functions which are typically applied in isogeometric analysis (IGA), see Reference 14. A comprehensive introduction to the topic of NURBS with many useful algorithms for their manipulation can be found in Reference 38. NURBS are based on B-Spline functions. Each B-Spline function is defined through a knot vector[†]

$$\Xi_p = \{\underbrace{0, \ \dots \ 0}_{p+1}, \underbrace{\xi_{p+2}, \ \dots \ , \xi_{n_{\text{ele}}+p+1}}_{n_{\text{ele}}-1}, \underbrace{1, \ \dots \ 1}_{p+1}\}, \tag{46}$$

where the index p denotes the polynomial degree of the shape function and n_{ele} the number of curve segments. The knot vector defines the number of finite elements as well as the smoothness of the basis. Knots in the interior with multiplicity $k > 1$ reduce the smoothness by C^{p-k}. Each unique entry defines the boundary of a finite element. Classically open knot vectors are employed in the IGA, which are defined by repeating the first and last entry $p+1$ times. In the case of open knot vectors, the basis functions are interpolatory at the beginning ($\xi = 0$) and the end ($\xi = 1$). Using the Cox-de-Boor recursive algorithm[14,38] a B-Spline basis can be computed via

$$\begin{aligned} \hat{N}_{i,0}(\xi) &= \begin{cases} 1 & \text{if } \xi_i \leq \xi < \xi_{i+1}, \\ 0 & \text{otherwise}, \end{cases} \\ \hat{N}_{i,p}(\xi) &= \frac{\xi - \xi_i}{\xi_{i+p} - \xi_i}\hat{N}_{i,p-1}(\xi) + \frac{\xi_{i+p+1} - \xi}{\xi_{i+p+1} - \xi_{i+1}}\hat{N}_{i+1,p-1}(\xi), \end{aligned} \tag{47}$$

where division by zero is defined as zero ($\frac{(\bullet)}{0} := 0$). The rational NURBS basis is constructed from

$$N_i(\xi) = \frac{\hat{N}_{i,p}(\xi) w_i}{W(\xi)} = \frac{\hat{N}_{i,p}(\xi) w_i}{\sum_{i=1}^{n_{\text{CP}}} N_{i,p}(\xi) w_i}, \tag{48}$$

where w_i is the ith weight of the ith control point. If all weights are set to one ($w_i = 1$) the NURBS basis coincides with the B-Spline basis. As already mentioned before, in the present work both Lagrange shape functions and NURBS shape functions are denoted as $N_i(\xi)$.

4.2 | Discrete strain measures

The discretized strain measures result from inserting the approximations (39) and (44) into the strain measures (27) and (29). Accordingly, strain measure (27) leads to the discrete counterpart

$$\mathbf{K}^h = 2\mathbf{G}(\mathbb{q}^h)\mathbb{q}^h_{,s}. \tag{49}$$

Inserting expression (40) for $\mathbb{q}^h_{,s}$ into (49) and taking into account $(16)_1$ eventually leads to the discretized strain measure

$$\mathbf{K}^h = \frac{2}{\left\|\mathbb{p}^h\right\|^2}\mathbf{G}(\mathbb{p}^h)\mathbb{p}^h_{,s}. \tag{50}$$

Similarly, the discretized version of strain measure (29) can be written in the form

$$\boldsymbol{\Gamma}^h = \frac{1}{\left\|\mathbb{p}^h\right\|^2}\mathbf{R}(\mathbb{p}^h)^\top\boldsymbol{\varphi}^h_{,s} - \mathbf{e}_3. \tag{51}$$

The discrete strain measures $\mathbf{K}^h$ and $\mathbf{\Gamma}^h$ inherit the frame-indifference of the underlying continuous strain measures, as will be shown below.

4.2.1 | Frame-indifference of the discrete strain measures

Similar to the continuous case, frame-indifference of the discrete strain measures can be shown by considering a superposed rigid motion of the discrete model of the beam. Despite the non-interpolatory nature of the NURBS basis, affine transformations of NURBS curves can be achieved by applying these transformations directly to the control points,[14] which is in complete analogy to the use of standard Lagrange shape functions. Correspondingly, a rigid motion of the control/nodal points is characterized by

$$\begin{aligned} \boldsymbol{\varphi}_i^{\#} &= \mathbf{R}(\mathbb{q})\boldsymbol{\varphi}_i + \mathbf{c}, \\ \mathbb{p}_i^{\#} &= \mathbb{r} \circ \mathbb{p}_i = \mathbf{Q}_l(\mathbb{r})\mathbb{p}_i. \end{aligned} \tag{52}$$

As before, $\mathbb{r} \in S^3$ represents an arbitrary rotation with associated rotation tensor $\mathbf{R}(\mathbb{r}) = \mathbf{E}(\mathbb{r})\mathbf{G}(\mathbb{r})^\top$. It can be easily verified that $(52)_2$ implies

$$\mathbb{p}^{h^{\#}} = \mathbb{r} \circ \mathbb{p}^h = \mathbf{Q}_l(\mathbb{r})\mathbb{p}^h \tag{53}$$

and

$$\left\| \mathbb{p}^{h^{\#}} \right\|^2 = \mathbb{p}^{h^{\#}} \cdot \mathbb{p}^{h^{\#}} = \mathbb{p}^h \cdot \mathbf{Q}_l(\mathbb{r})^\top \mathbf{Q}_l(\mathbb{r})\mathbb{p}^h = \mathbb{p}^h \cdot \mathbb{p}^h = \left\| \mathbb{p}^h \right\|^2, \tag{54}$$

where $\mathbf{Q}_l(\mathbb{r})^\top \mathbf{Q}_l(\mathbb{r}) = \mathbf{I}_4$ has been used. Now (50) gives rise to

$$\begin{aligned} \mathbf{K}^{h^{\#}} &= \frac{2}{\left\| \mathbb{p}^{h^{\#}} \right\|^2} \mathbf{G}(\mathbb{p}^{h^{\#}}) \mathbb{p}_{,s}^{h^{\#}} \\ &= \frac{2}{\left\| \mathbb{p}^h \right\|^2} \mathbf{G}(\mathbb{r} \circ \mathbb{p}^h) \mathbf{Q}_l(\mathbb{r}) \mathbb{p}_{,s}^h. \end{aligned} \tag{55}$$

It can be verified by a straightforward calculation that the identity

$$\mathbf{G}(\mathbb{r} \circ \mathbb{p}^h) = \mathbf{G}(\mathbb{p}^h)\mathbf{Q}_l(\mathbb{r})^\top \tag{56}$$

holds. Using the last equation along with the orthogonality of $\mathbf{Q}_l(\mathbb{r})$ leads to the result $\mathbf{K}^{h^{\#}} = \mathbf{K}^h$, which confirms the invariance of the discrete strain measure $\mathbf{K}^h$ under rigid motions. Similarly, we consider

$$\mathbf{\Gamma}^{h^{\#}} = \frac{1}{\left\| \mathbb{p}^{h^{\#}} \right\|^2} \mathbf{R}(\mathbb{p}^{h^{\#}})^\top \boldsymbol{\varphi}_{,s}^{h^{\#}} - \mathbf{e}_3, \tag{57}$$

where (44) together with $(52)_1$ implies

$$\boldsymbol{\varphi}_{,s}^{h^{\#}} = \mathbf{R}(\mathbb{r}) \sum_{i=1}^{n} N_{i,s} \boldsymbol{\varphi}_i + \mathbf{c} \sum_{i=1}^{n} N_{i,s} = \mathbf{R}(\mathbb{r}) \boldsymbol{\varphi}_{,s}^h. \tag{58}$$

Here, the partition of unity property $\sum_{i=1}^{n} N_i = 1$ has been used which holds for both the NURBS and the Lagrange shape functions. We thus obtain

$$\mathbf{\Gamma}^{h^{\#}} = \frac{1}{\left\| \mathbb{p}^h \right\|^2} \mathbf{R}(\mathbb{r} \circ \mathbb{q}^h)^\top \mathbf{R}(\mathbb{r}) \boldsymbol{\varphi}_{,s}^h. \tag{59}$$

Since the identity

$$\mathbf{R}(\mathbb{r} \circ \mathbb{p}) = \mathbf{R}(\mathbb{r})\mathbf{R}(\mathbb{p}) \tag{60}$$

holds for any $\mathbb{p} \in \mathbb{H}$, we eventually obtain

$$\begin{aligned} \boldsymbol{\Gamma}^{h^\#} &= \frac{1}{\|\mathbb{p}^h\|^2}\mathbf{R}(\mathbb{p}^h)^\top \mathbf{R}(\mathbb{r})^\top \mathbf{R}(\mathbb{r})\boldsymbol{\varphi}_{,s}^h \\ &= \frac{1}{\|\mathbb{p}^h\|^2}\mathbf{R}(\mathbb{p}^h)^\top \boldsymbol{\varphi}_{,s}^h \\ &= \boldsymbol{\Gamma}^h \end{aligned} \tag{61}$$

which corroborates the frame-indifference of the discrete strain measure $\boldsymbol{\Gamma}^h$.

4.3 | Discrete weak form

The finite element formulation essentially follows from inserting the finite element approximations described above into weak form (34). Although we ensure that $(\mathbb{q}^h, \delta\mathbb{q}^h) \in TS^3$ for all $s \in [0, L]$ from the outset, we still have to take care of the redundancy of $(\mathbb{p}_i, \delta\mathbb{p}_i) \in \mathbb{H} \times \mathbb{H}$. In essence, this redundancy occurs due to the fact that the quaternion variables in the control/nodal points belong to a 4-dimensional space, whereas $\dim(S^3) = 3$. To account for the redundancy, we impose the unit-length constraint on the quaternion field $\mathbb{p}^h \in \mathbb{H}$ by applying the method of Lagrange multipliers. Accordingly, we introduce the discretized weak form

$$G_{\text{int}}(\boldsymbol{\varphi}^h, \mathbb{q}^h; \delta\boldsymbol{\varphi}^h, \delta\mathbb{q}^h) + G_\lambda(\mathbb{p}^h, \lambda^h; \delta\mathbb{p}^h) = G_{\text{ext}}(\boldsymbol{\varphi}^h, \mathbb{q}^h; \delta\boldsymbol{\varphi}^h, \delta\mathbb{q}^h), \tag{62}$$

where G_{int} and G_{ext} are given by (37) and (38), respectively. Furthermore, G_λ accounts for the unit-length constraint on $\mathbb{p}^h \in \mathbb{H}$. In this connection, λ^h represent the contribution of the Lagrange multipliers. Two alternative versions of G_λ will be introduced in Section 4.3.3.

4.3.1 | Contribution of the internal forces

The contribution of the internal forces to the weak form, G_{int} in (62), can be obtained by starting from the continuous expression for G_{int}, (37), and making use of (39), (40) and (42). Accordingly, a straightforward calculation yields

$$\begin{aligned} G_{\text{int}}^h(\boldsymbol{\varphi}^h, \mathbb{p}^h; \delta\boldsymbol{\varphi}^h, \delta\mathbb{p}^h) = \int_0^L &\left(\delta\boldsymbol{\varphi}_{,s}^h \cdot \mathbf{E}(\mathbb{q}^h) + \frac{2}{\|\mathbb{p}^h\|}\boldsymbol{\varphi}_{,s}^h \cdot \mathbf{E}(\delta\mathbb{p}^h)\right)\mathbf{G}(\mathbb{q}^h)^\top \mathbf{N}^h \\ &- \delta\mathbb{p}^h \cdot \frac{2}{\|\mathbb{p}^h\|^2}\left[\left(\mathbb{p}^h \otimes \mathbf{R}(\mathbb{q}^h)^\top \boldsymbol{\varphi}_{,s}^h\right)\mathbf{N}^h + 2\left(\mathbb{q}^h \otimes \mathbf{G}(\mathbb{q}^h)\mathbb{p}_{,s}^h\right)\mathbf{M}^h\right] \\ &+ \frac{2}{\|\mathbb{p}^h\|^2}\left(\delta\mathbb{p}_{,s}^h \cdot \mathbf{G}(\mathbb{p}^h)^\top - \delta\mathbb{p}^h \cdot \mathbf{G}(\mathbb{p}_{,s}^h)^\top\right)\mathbf{M}^h \mathrm{d}s. \end{aligned} \tag{63}$$

Here, $\mathbf{N}^h = \mathbf{D}_1\boldsymbol{\Gamma}^h$ and $\mathbf{M}^h = \mathbf{D}_2\mathbf{K}^h$, where the discrete strain measures are given by (50) and (51). The last equation can also be written in the form

$$G_{\text{int}}^h(\boldsymbol{\varphi}_i, \mathbb{p}_i; \delta\boldsymbol{\varphi}_i, \delta\mathbb{p}_i) = \sum_{i=1}^n \begin{bmatrix} \delta\boldsymbol{\varphi}_i \\ \delta\mathbb{p}_i \end{bmatrix}^\top \int_0^L \begin{bmatrix} \mathbf{B}_{\boldsymbol{\varphi}\boldsymbol{\varphi}}^{i^\top} & 0 \\ \mathbf{B}_{\mathbb{p}\boldsymbol{\varphi}}^{i^\top} & \mathbf{B}_{\mathbb{p}\mathbb{p}}^{i^\top} \end{bmatrix} \begin{bmatrix} \mathbf{N}^h \\ \mathbf{M}^h \end{bmatrix} \mathrm{d}s, \tag{64}$$

where the nodal operator matrices are given by

$$\begin{aligned}
\mathbf{B}^i_{\varphi\varphi} &= N_{i,s}\mathbf{R}(\mathbb{q}^h)^\top \\
\mathbf{B}^i_{\mathbb{p}\varphi} &= \frac{2N_i}{\left\|\mathbb{p}^h\right\|^2}\left(\mathbf{G}(\mathbb{p}^h)^\top \overset{+}{\boldsymbol{\varphi}}{}^h_{,s} - \mathbf{R}(\mathbb{q}^h)^\top \boldsymbol{\varphi}^h_{,s} \otimes \mathbb{p}^h\right) \\
\mathbf{B}^i_{\mathbb{p}\mathbb{p}} &= \frac{2}{\left\|\mathbb{p}^h\right\|^2}\left[N_{i,s}\mathbf{G}(\mathbb{p}^h) - N_i\left(\mathbf{G}(\mathbb{p}^h_{,s}) + 2\mathbf{G}(\mathbb{q}^h)\mathbb{p}^h_{,s} \otimes \mathbb{q}^h\right)\right].
\end{aligned} \tag{65}$$

Note that in $(65)_2$ use has been made of the notation introduced in (18). An alternative form of (64) is given by

$$G^h_{\text{int}}(\boldsymbol{\varphi}_i, \mathbb{p}_i; \delta\boldsymbol{\varphi}_i, \delta\mathbb{p}_i) = \sum_{i=1}^{n}\left(\delta\boldsymbol{\varphi}_i \cdot \mathbf{f}^{\varphi,i}_{\text{int}} + \delta\mathbb{p}_i \cdot \mathbf{f}^{\mathbb{p},i}_{\text{int}}\right), \tag{66}$$

where

$$\begin{aligned}
\mathbf{f}^{\varphi,i}_{\text{int}} &= \int_0^L \mathbf{B}^{i^\top}_{\varphi\varphi}\mathbf{N}^h \mathrm{d}s \\
\mathbf{f}^{\mathbb{p},i}_{\text{int}} &= \int_0^L \mathbf{B}^{i^\top}_{\mathbb{p}\boldsymbol{\varphi}}\mathbf{N}^h + \mathbf{B}^{i^\top}_{\mathbb{p}\mathbb{p}}\mathbf{M}^h \mathrm{d}s
\end{aligned} \tag{67}$$

denote the internal forces corresponding to the control/nodal points.

Remark 1. Expression G^h_{int} in (63) can also be obtained by starting from

$$G^h_{\text{int}}(\boldsymbol{\varphi}^h, \mathbb{p}^h; \delta\boldsymbol{\varphi}^h, \delta\mathbb{p}^h) = \int_0^L \delta\boldsymbol{\Gamma}^h \cdot \mathbf{N}^h + \delta\mathbf{K}^h \cdot \mathbf{M}^h \mathrm{d}s \tag{68}$$

and taking into account the discrete strain measures (50) and (51).

4.3.2 | Contribution of the external loading

The contribution of the external loading to the weak form follows from (38) by taking into account (42) and (45). Accordingly, we obtain

$$G^h_{\text{ext}}(\boldsymbol{\varphi}^h, \mathbb{p}^h; \delta\boldsymbol{\varphi}^h, \delta\mathbb{p}^h) = \int_0^L \delta\boldsymbol{\varphi}^h \cdot \overline{\mathbf{n}} + \delta\mathbb{p}^h \cdot \frac{2}{\left\|\mathbb{p}^h\right\|}\mathbf{E}(\mathbb{q}^h)^\top\overline{\mathbf{m}}\,\mathrm{d}s \tag{69}$$

leading to

$$G^h_{\text{ext}}(\boldsymbol{\varphi}_i, \mathbb{p}_i; \delta\boldsymbol{\varphi}_i, \delta\mathbb{p}_i) = \sum_{i=1}^{n}\left(\delta\boldsymbol{\varphi}_i \cdot \mathbf{f}^{\varphi,i}_{\text{ext}} + \delta\mathbb{p}_i \cdot \mathbf{f}^{\mathbb{p},i}_{\text{ext}}\right), \tag{70}$$

where

$$\begin{aligned}
\mathbf{f}^{\varphi,i}_{\text{ext}} &= \int_0^L N_i\overline{\mathbf{n}}\,\mathrm{d}s \\
\mathbf{f}^{\mathbb{p},i}_{\text{ext}} &= \int_0^L \frac{2N_i}{\left\|\mathbb{p}^h\right\|}\mathbf{E}(\mathbb{q}^h)^\top\overline{\mathbf{m}}\,\mathrm{d}s
\end{aligned} \tag{71}$$

denote the discrete external forces corresponding to the control/nodal points.

4.3.3 | Contribution of the unit-length constraints

As outlined above we impose the unit-length constraint on the quaternions to resolve the redundancy of the quaternions at the control/nodal points. To this end we investigate two alternative procedures for imposing the unit-length constraint

$$g(\mathbb{p}) = \frac{1}{2}(\mathbb{p} \cdot \mathbb{p} - 1) = 0 \tag{72}$$

on the quaternion field. While the first option imposes the unit-length constraint in weak form, the second option is based on a strong (or point-wise) imposition at the control/nodal points.

Weak enforcement

The weak imposition of the constraint (72) yields the following contribution of the conjugate constraint forces to the weak form

$$\begin{aligned} G^h_\lambda(\mathbb{p}^h, \lambda^h; \delta\mathbb{p}^h) &= \int_0^L \delta g(\mathbb{p}^h)\lambda^h \mathrm{d}s \\ &= \int_0^L \delta\mathbb{p}^h \cdot \mathbb{p}^h \lambda^h \mathrm{d}s. \end{aligned} \tag{73}$$

In addition to that, the weak enforcement of the unit-length constraint is based on the condition

$$\int_0^L \delta\lambda^h g(\mathbb{p}^h)\mathrm{d}s = 0. \tag{74}$$

Concerning the discretization of the Lagrange multiplier field we apply a Bubnov–Galerkin approach which applies the same NURBS/Lagrangian shape functions as before. Accordingly,

$$\lambda^h(s) = \sum_{i=1}^n N_i(s)\lambda_i \quad \text{and} \quad \delta\lambda^h(s) = \sum_{i=1}^n N_i(s)\delta\lambda_i. \tag{75}$$

Making use of these ansatz functions in (74) and (73) yields the discrete constraint functions

$$g_i = \int_0^L N_i g(\mathbb{p}^h)\mathrm{d}s = 0 \tag{76}$$

for $i = 1, \dots, n$, together with the contribution to the weak form of the discrete constraint forces

$$G^h_\lambda(\mathbb{p}_i, \lambda_i; \delta\mathbb{p}_i) = \sum_{i=1}^n \delta\mathbb{p}_i \cdot \mathbf{f}^i_\lambda, \tag{77}$$

where the discrete constraint forces corresponding to the control/nodal points are given by

$$\mathbf{f}^{\mathbb{p},i}_\lambda = \int_0^L N_i \mathbb{p}^h \lambda^h \mathrm{d}s. \tag{78}$$

Strong enforcement

To account for the redundancy of the quaternions $\mathbb{p}_i \in \mathbb{H}^4$, the unit-length constraint can also be enforced directly at the control/nodal points. In this case, the discrete constraints are given by

$$g_i = g(\mathbb{p}_i) = \frac{1}{2}(\mathbb{p}_i \cdot \mathbb{p}_i - 1) = 0 \tag{79}$$

for $i = 1, \dots, n$. The contribution of the conjugate constraint forces to the weak form can again be written in the form (77) where

$$\mathbf{f}_{\lambda}^{\mathbb{p},i} = \mathbb{p}_i \lambda_i \tag{80}$$

denote the constraint forces corresponding to the control/nodal points.

4.3.4 | Algebraic system of equations

To summarize the discretization procedure described above, weak form (62) eventually yields

$$\sum_{i=1}^{n} \begin{bmatrix} \delta\boldsymbol{\varphi}_i \\ \delta\mathbb{p}_i \\ \delta\lambda_i \end{bmatrix}^{\mathsf{T}} \left(\begin{bmatrix} \mathbf{f}_{\text{int}}^{\varphi,i} \\ \mathbf{f}_{\text{int}}^{\mathbb{p},i} \\ 0 \end{bmatrix} + \begin{bmatrix} 0 \\ \mathbf{f}_{\lambda}^{\mathbb{p},i} \\ g_i \end{bmatrix} - \begin{bmatrix} \mathbf{f}_{\text{ext}}^{\varphi,i} \\ \mathbf{f}_{\text{ext}}^{\mathbb{p},i} \\ 0 \end{bmatrix} \right) = 0 \tag{81}$$

which has to hold for arbitrary $(\delta\boldsymbol{\varphi}_i, \delta\mathbb{p}_i, \delta\lambda_i) \in \mathbb{R}^3 \times \mathbb{H} \times \mathbb{R}$ $(i = 1, \dots, n)$. One may either apply the strong or the weak enforcement of the constraints described in Section 4.3.3. To solve the algebraic system of nonlinear equations we apply Newton's method. Accordingly, in each Newton iteration a saddle point system has to be solved in order to eventually determine $(\boldsymbol{\varphi}_i, \mathbb{p}_i, \lambda_i) \in \mathbb{R}^3 \times \mathbb{H} \times \mathbb{R}$ $(i = 1, \dots, n)$. In this connection a standard additive update procedure is applied in each Newton iteration.

4.3.5 | Elimination of the Lagrange multipliers and the constraints

The strong enforcement of the constraints makes possible to apply a simple procedure for the elimination of the discrete constraint forces along with the constraints. This approach is referred to as the discrete null space method.[33,39,40] The discrete null space method essentially relies on two steps. Starting from the algebraic constraint (79), the corresponding consistency condition $\delta g_i = \mathbb{p}_i \cdot \delta\mathbb{p}_i = 0$ can be identically fulfilled by choosing $\delta\mathbb{p}_i = \mathbf{G}(\mathbb{p}_i)^{\mathsf{T}} \delta\boldsymbol{\theta}_i$ for any $\delta\boldsymbol{\theta}_i \in \mathbb{R}^3$. The last relationship for $\delta\mathbb{p}_i$ can be inserted into (81) to annihilate the constraint forces since

$$\left(\mathbf{G}(\mathbb{p}_i)^{\mathsf{T}} \delta\boldsymbol{\theta}\right) \cdot \mathbf{f}_{\lambda}^{\mathbb{p},i} = \delta\boldsymbol{\theta}_i \cdot \mathbf{G}(\mathbb{p}_i) \mathbf{f}_{\lambda}^{\mathbb{p},i} = \delta\boldsymbol{\theta}_i \cdot \mathbf{G}(\mathbb{p}_i) \mathbb{p}_i \lambda_i = 0$$

for arbitrary $\delta\boldsymbol{\theta} \in \mathbb{R}^3$ due to $(16)_1$. Accordingly, (81) can be recast in the size-reduced form

$$\sum_{i=1}^{n} \begin{bmatrix} \delta\boldsymbol{\varphi}_i \\ \delta\boldsymbol{\theta}_i \end{bmatrix}^{\mathsf{T}} \left(\begin{bmatrix} \mathbf{f}_{\text{int}}^{\varphi,i} \\ \mathbf{G}(\mathbb{p}_i) \mathbf{f}_{\text{int}}^{\mathbb{p},i} \end{bmatrix} - \begin{bmatrix} \mathbf{f}_{\text{ext}}^{\varphi,i} \\ \mathbf{G}(\mathbb{p}_i) \mathbf{f}_{\text{ext}}^{\mathbb{p},i} \end{bmatrix} \right) = 0 \tag{82}$$

which has to hold for arbitrary $(\delta\boldsymbol{\varphi}_i, \delta\boldsymbol{\theta}_i) \in \mathbb{R}^3 \times \mathbb{R}^3$ $(i = 1, \dots, n)$. Of course, the constraints (79), that is, $g_i = 0$, still have to be satisfied. However, in a second step we make these constraints obsolete by replacing the redundant unknowns $\mathbb{p}_i \in \mathbb{H}$ with new unknowns $\boldsymbol{\theta}_i \in \mathbb{R}^3$ such that

$$\mathbb{p}_i = \exp_{S^3}\left(\left(0, \frac{1}{2}\boldsymbol{\theta}_i\right)\right) \circ \mathbb{p}_i^0, \tag{83}$$

where $\exp_{S^3} : T_{\mathbb{p}_i^0} S^3 \mapsto S^3$ denotes the exponential map on S^3. Provided that the reference value $\mathbb{p}_i^0 \in S^3$, the update formula ensures $\mathbb{p}_i \in S^3$ so that the unit-length constraint is automatically satisfied. In equilibrium problems, $\mathbb{p}_i^0 \in S^3$ may be chosen to coincide with the last equilibrium configuration. Then, the application of a new load increment yields a new equilibrium configuration which is characterized by the rotation increments $\boldsymbol{\theta}_i \in \mathbb{R}^3$. During a load step the incremental rotations $\boldsymbol{\theta}_i$ are updated additively. Further details of the discrete null space method in the context of unit quaternions can be found in Reference 34.

5 | NUMERICAL EXAMPLES

In this section, we present several numerical examples to examine the numerical performance of alternative element formulations. In particular, we investigate to what extend the quaternion projection (39) does improve the performance when compared to the 'classical' quaternion discretization based on

$$\mathbb{p}^h(s) = \sum_{i=1}^{n} N_i(s)\mathbb{p}_i \tag{84}$$

The classical discretization can be easily realized by skipping the projection in (39). Furthermore, we impose the unit-length condition on the quaternions either in weak or in strong form, as described in Section 4.3.3. Last but not least we compare the NURBS-based formulation with that based on Lagrange shape functions.

To distinguish between the alternative formulations we introduce the abbreviations summarized in Tables 1 and 2. For example, NPS3 means the NURBS-based formulation of order three relying on the projection (39) and the strong enforcement of the unit-length constraint (79). Similarly, LCS2 means the Lagrange element of order two based on the classical approximation (84) and the strong enforcement of the unit-length constraint (79).

Concerning the initialization of the quaternions in the control points of the NURBS-based elements, we first compute auxiliary director frames at the Gauss points from which unit-quaternions can be extracted by applying Spurrier's algorithm.[41] Subsequently, the unit quaternions in the control points are calculated by applying the procedure originally proposed in Reference 42 in the context of shells. Due to the interpolatory nature of the Lagrange shape functions, the initial director frames can be directly set up at the nodes. Application of Spurrier's algorithm directly yields the nodal quaternions.

TABLE 1 Abbreviations for elements based on NURBS shape functions.

Shape functions	Projection	Constraints	Order	Abbreviation
NURBS	Yes	Strong	1	NPS1
NURBS	Yes	Strong	2	NPS2
NURBS	Yes	Strong	3	NPS3
NURBS	Yes	Weak	1	NPW1
NURBS	Yes	Weak	2	NPW2
NURBS	Yes	Weak	3	NPW3
NURBS	No	Strong	1	NCS1
NURBS	No	Strong	2	NCS2
NURBS	No	Strong	3	NCS3
NURBS	No	Weak	1	NCW1
NURBS	No	Weak	2	NCW2
NURBS	No	Weak	3	NCW3

TABLE 2 Abbreviations for elements based on Lagrange shape functions.

Shape functions	Projection	Constraints	Order	Abbreviation
Lagrange	Yes	Strong	1	LPS1
Lagrange	Yes	Strong	2	LPS2
Lagrange	Yes	Strong	3	LPS3
Lagrange	No	Strong	1	LCS1
Lagrange	No	Strong	2	LCS2
Lagrange	No	Strong	3	LCS3

To eliminate transverse shear locking we apply selectively reduced numerical integration. In particular, we choose the number of Gauss points equal to the element order.

The mesh refinement for the NURBS-based elements was performed with the algorithm proposed in Reference 43, to keep the Jacobian of the isoparametric transformation constant over the domain. The mesh refinement for the Lagrange elements was performed by using an equidistant distribution of the finite element nodes.

5.1 | Cantilever beam under end moment

The first example deals with the well-known bench mark problem of an initially straight cantilever beam, which is deformed into a circle by an end moment, while being fixed on the other end. A sketch of the problem is shown in Figure 2. The beam has length L and $\overline{\mathbf{m}}$ is an external torque applied at the right end of the beam given by $\overline{\mathbf{m}} = M\mathbf{e}_3$. The corresponding contribution to the weak form in the present beam formulation is provided in Appendix B. For $M = 2\pi\frac{EI}{L}$ the beam forms a complete circle, where EI is the bending stiffness of the beam. The beam has an initial length of $L = 1$ and the following stiffness parameters $GA = 1/270$, $EA = 1/100$, $EI = 1/12 * 1 \times 10^{-4}$ and $GI_\mathrm{p} = 1/6 * 1 \times 10^{-4}$.

The total load is applied in 10 equally spaced incremental steps. As convergence criteria of the Newton solver $\|\mathbf{R}\| = 1 \times 10^{-12}$ is used, where $\|\mathbf{R}\|$ is the 2-norm of the residual vector. The error measure is defined as $e = \left\|\boldsymbol{\varphi}_\mathrm{num}(s = L)\right\|$, where $\boldsymbol{\varphi}_\mathrm{num}(s = L)$ is the placement of the tip of the numerical model.

The convergence behavior is shown in Figure 3 for various element formulations under consideration. In particular, Figure 3A shows the results for NURBS shape functions of order $p = 1, \ldots, 3$. Accordingly, the projection-based approach shows the best convergence behavior for both the strong enforcement of the unit-length constraint (NPSp, $p = 1, \ldots, 3$) and the weak enforcement (NPWp, $p = 1, \ldots, 3$). In both cases the rate of convergence turns out to be $\mathcal{O}(h^{2p})$.

However, if the projection is skipped the results worsen significantly if the strong enforcement of the unit-length constraint is used (Figure 3A, NCSp, $p = 1, \ldots, 3$). In particular, the order of convergence does not improve with increased order of the NURBS shape functions but stays at a level of $\mathcal{O}(h^2)$. This can be explained by the non-interpolatory nature of NURBS shape functions. Thus, enforcing the unit-length constraint at the control points in general does not imply unit-length of the quaternion discretization inside the computational domain. Still considering the classical interpolation (without projection) but choosing the weak enforcement instead of the strong enforcement of the unit-length constraint improves the convergence results (see NCWp, $p = 1, \ldots, 3$, Figure 3A).

It is also worth mentioning that the projection-based formulation in general exhibits a superior convergence behavior in the iterative solution procedure, in the sense that coarser meshes still reach a solution. In particular, while the projection-based formulation reaches a solution for the coarse discretization with 8 elements, this is not the case for the classical formulation which requires more than 8 elements to reach converged results (cf. Figure 3A).

We now turn to the convergence results of the elements based on the Lagrange shape functions (Figure 3B) where we focus our attention to the strong nodal enforcement of the unit-length constraint. Accordingly, the projection-based formulation (LPSp, $p = 1, \ldots, 3$) again shows superior convergence of order $\mathcal{O}(h^{2p})$, in analogy to the NURBS-based case. The classical formulation (LCSp, $p = 1, \ldots, 3$) again shows an order reduction, which, however, is not as pronounced as in the case of NURBS shape function. Specifically, for Lagrange elements the order reduction is deferred to $p \geq 3$. This slightly improved convergence behavior presumably is caused by the interpolatory nature of Lagrange polynomials.

The deformed configurations of the beam corresponding to five different load levels are shown in Figure 4. As expected, a complete roll-up takes place for $M = 2\pi\frac{EI}{L}$.

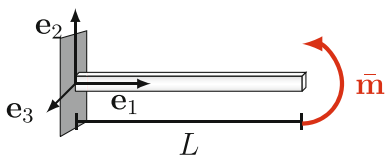

FIGURE 2 Sketch of a cantilever beam with an end torque.

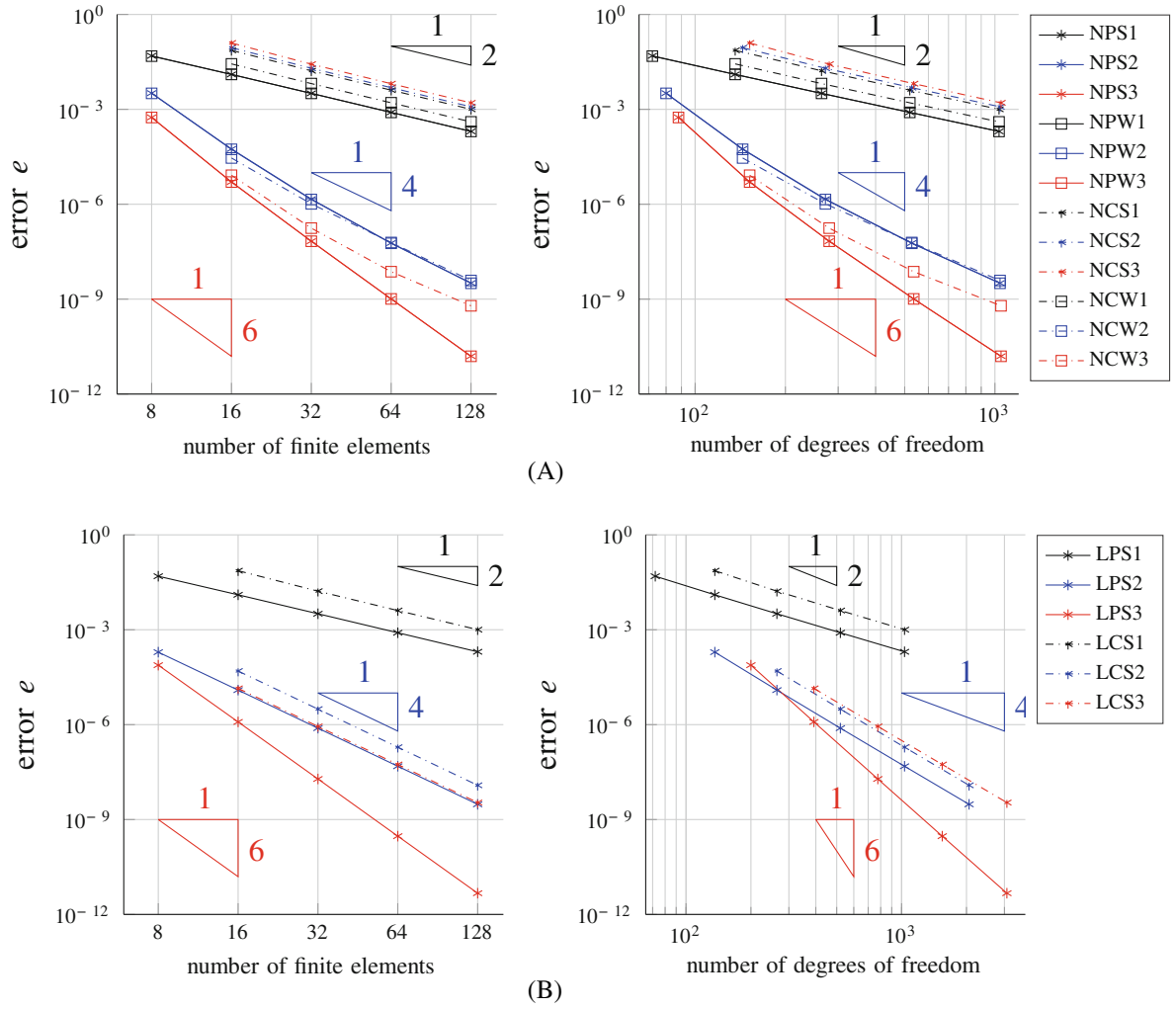

FIGURE 3 Convergence behavior of the quaternion beam formulation for the roll-up into a circle. (A) Convergence behavior for the isogeometric analysis. (B) Convergence behavior for the Lagrange elements.

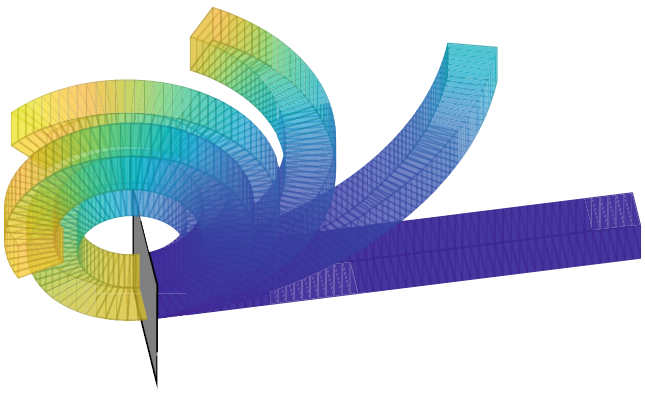

FIGURE 4 Snapshots of the roll-up movement of the cantilever beam (32 NPS3 elements) for the load levels $M = 0$, $\frac{1}{5}M$, $\frac{2}{5}M$, $\frac{3}{5}M$, $\frac{4}{5}M$, $M = 2\pi\frac{EI}{L}$.

5.2 | 3D bending and twist

This example is taken from Reference 36. It consists of an initially straight beam clamped at one end and loaded at the other end with a torque, which is applied in 250 load steps. The torque is applied in such a way that the beam forms a helix with two complete coils. The helix has a radius of $R_0 = 10$ and a height of $h = 50$. The applied torque is given by

$$\overline{\mathbf{m}} = \left(m^1 \mathbf{d}_1 + m^3 \mathbf{d}_3\right)$$

where $m^1 = -4R_0 \frac{\pi^3 r^4}{L^2}$ and $m^3 = \frac{\pi^2 h r^4}{L^2}$. The corresponding contribution to the weak form of the present beam formulation is provided in Appendix B. The initial length of the beam is given by $L = \sqrt{1+c^2} R_0 4\pi$, where $c = \frac{h}{4R_0\pi}$. A slenderness ration ζ is used to define the radius of the beam $r = \frac{L}{2\zeta}$. The beam stiffness parameters are given by $GA = \frac{1}{2}\pi r^2$, $EA = \pi r^2$, $EI = \frac{\pi}{4} r^4$ and $GI_\mathrm{p} = \frac{\pi}{2} r^4$. The straight initial configuration is defined through

$$\boldsymbol{\varphi}(s) = -R_0 \mathbf{e}_2 + s\mathbf{d}_3^0,$$

where $s \in [0, L]$, and the initial director frame is given by

$$\mathbf{d}_1^0 = R_0\alpha(c\mathbf{e}_1 - \mathbf{e}_3) \qquad \mathbf{d}_2^0 = \mathbf{e}_2 \qquad \mathbf{d}_3^0 = R_0\alpha(\mathbf{e}_1 + c\mathbf{e}_3),$$

where $\alpha = \frac{4\pi}{L}$.

Figure 5 shows three deformed configurations of the beam corresponding to three different load levels. In Figure 6 the convergence behavior of the alternative beam elements under consideration is shown for a slenderness ratio of $\zeta = 25$. The error measure plotted is given by $e = \frac{\|\boldsymbol{\varphi}_{\mathrm{num}}(s=L) - \boldsymbol{\varphi}_{\mathrm{ana}}(s=L)\|}{\|\boldsymbol{\varphi}_{\mathrm{num}}(s=L)\|}$, where $\boldsymbol{\varphi}_{\mathrm{ana}}(s=L)$ is the analytical solution for the displacement of the tip under the final external torque $\overline{\mathbf{m}}$.

The convergence behavior is in complete analogy to that of the previous example. Accordingly, the projection-based approach yields superior convergence rates of $\mathcal{O}(h^{2p})$, together with a more robust solution behavior, in the sense that already 16 elements suffice to yield convergence of the iterative solution procedure. In contrast to that, the classical formulation (without projection) requires more elements to yield converged results. In addition to that, the classical formulation again exhibits order reduction for $p \geq 2$, which is especially pronounced for NCS2 and NCS3.

5.3 | Numerical path-independence test

As mentioned in Section 1, early discretization approaches of the geometrically exact beam model were neither frame-indifferent nor path-independent. The frame-indifference of the present formulation was shown in Section 4. With

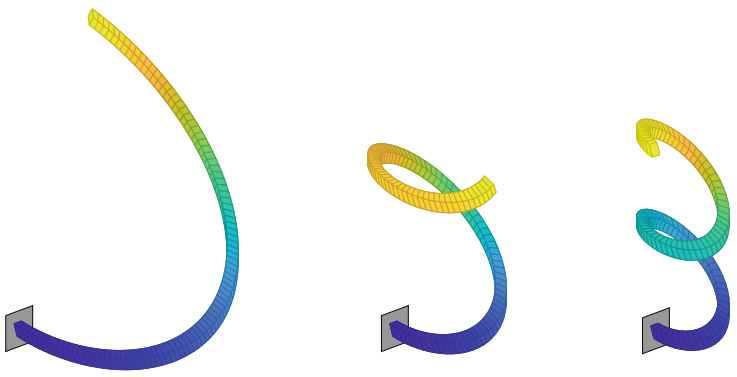

FIGURE 5 Configurations of the deformed beam corresponding to different numbers of load steps. Eventually, a helix with two complete coils is reached. (A) Load level: $\frac{8}{25}\,\overline{\mathbf{m}}$ – 80 loads steps. (B) Load level: $\frac{16}{25}\,\overline{\mathbf{m}}$ – 160 load steps. (C) Load level: $\overline{\mathbf{m}}$ – 250 load steps.

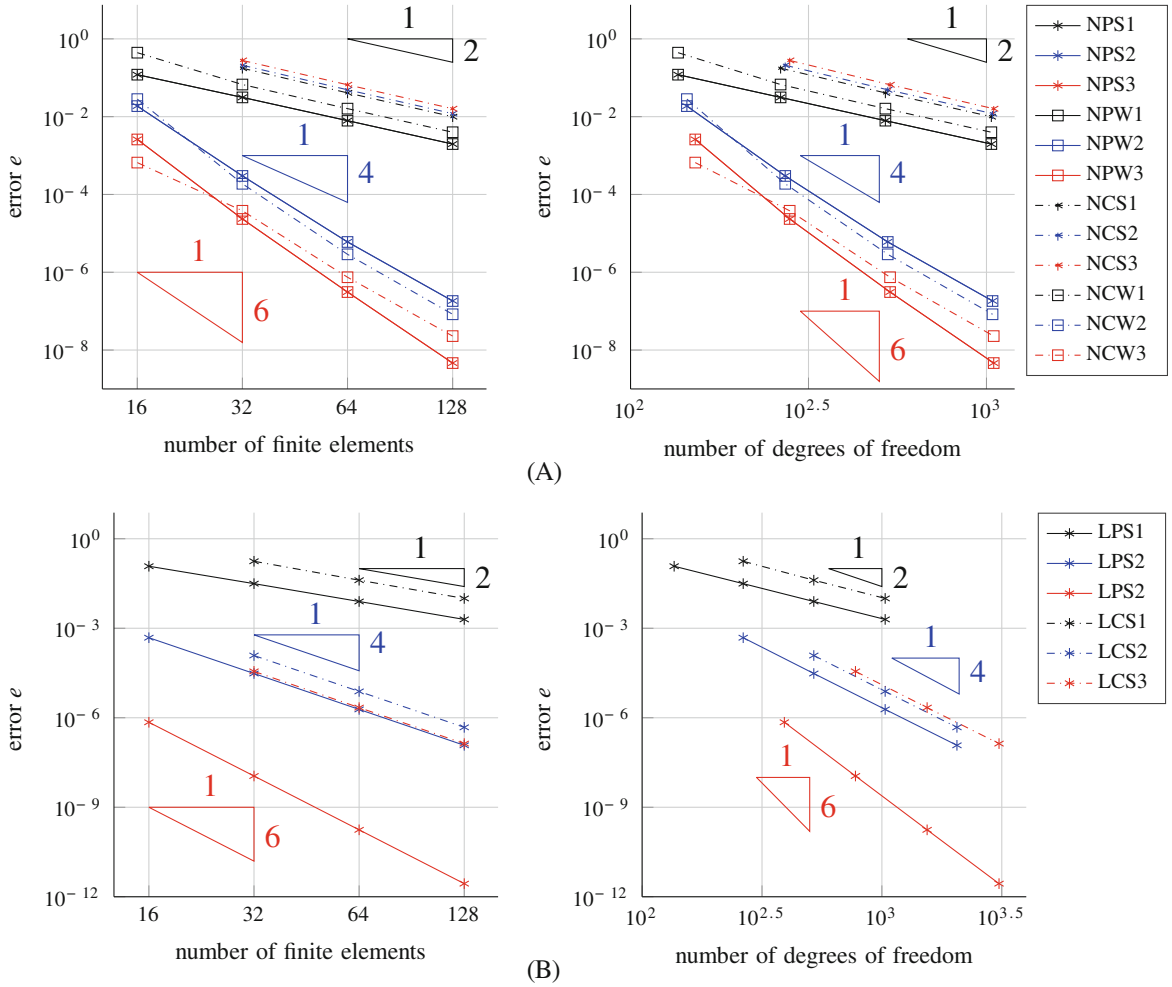

FIGURE 6 Convergence behavior of the quaternion beam formulation. (A) Convergence behavior for the isogeometric analysis. (B) Convergence behavior for the Lagrange elements.

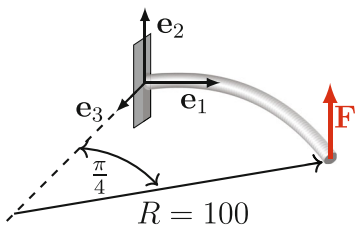

FIGURE 7 Sketch of 3D cantilever beam with an applied point force.

this example we verify that the proposed quaternion formulation is also path-independent. As shown in Figure 7, the initial configuration corresponds to a curved beam forming 1/8th of a circle in the $\mathbf{e}_1 - \mathbf{e}_3$ plane. The circle has a radius of 100.

An external force $\mathbf{F} = F_i \mathbf{e}_i$ is applied in a loading cycle at the tip of the beam. Specific values of the loading cycle are shown in Table 3. The cycle begins with a force of $\mathbf{F} = \mathbf{0}$. The load level is than varied with $\|\mathbf{F}\| = 25$ in each load step. This results in a total of 144 load steps. In the last load step the force is removed so that the initial configuration should be obtained again. The beam's stiffness parameters are given by $GA = 5 \times 10^6$, $EA = 1 \times 10^7$ and $EI = GI_p = 1/12 * 1 \times 10^7$. The convergence criteria for the Newton method is set to $\|\mathbf{R}\| = 1 \times 10^{-6}$.

TABLE 3 Numerical path-independence test: tip displacement in 2-direction corresponding to specific load levels.

	Tip displacement in 2-direction		
Load level	**Δθ formulation[8]**	**Lagrange (LPS1)**	**NURBS (NPS1)**
$[F_1,\ F_2,\ F_3]$	**32 el. $p = 1$**	**32 el. $p = 1$**	**32 el. $p = 1$**
$[0\ 0\ 0]$	0	0	0
$[-600\ 0\ 0]$	0	-8.8844×10^{-20}	-2.3202×10^{-14}
$[-600\ 600\ 0]$	59.7884	59.8262	59.8796
$[-600\ 600\ 600]$	38.6655	38.6875	38.6952
$[0\ 600\ 600]$	37.5087	37.5269	37.5247
$[0\ 0\ 600]$	0.0190	-1.6362×10^{-11}	-1.6369×10^{-11}
$[0\ 0\ 0]$	0.0374	1.2632×10^{-23}	-7.8410×10^{-16}

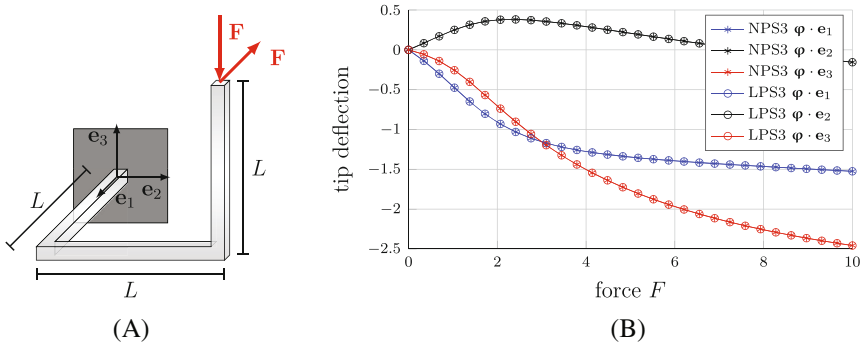

FIGURE 8 Beam patches with slope discontinuity. (A) Sketch of the problem. (B) Deflection of the tip versus force.

The results obtained with 32 linear elements are displayed in Table 3. For comparison, the results of the '**Δθ** formulation' taken from Reference 8 are also shown. This formulation goes back to Reference 2 and is known to be path-dependent.[20] Further results obtained with varying number of elements and different element orders can be found in Appendix C (Tables C1–C6). All the results have been obtained with a strong enforcement of the unit-length constraint.

In contrast to the path-dependent **Δθ** formulation, which does not return to the $\mathbf{e}_1 - \mathbf{e}_3$ plane, both quaternion formulations under investigation turn back to the initial configuration after the load has been removed (up to numerical round-off), which verifies their path-independence.

5.4 | Beam patches with slope discontinuity

In this example we investigate the capability of the present formulation to deal with discontinuities of the reference curve of the beam. This example has been treated previously in References 36,44,45. The initial geometry is shown in Figure 8A. It consists of three beam segments with the length $L = 1$, which are connected rigidly at a 90° angel.

The rigid intersection of the beam segments can be either formulated by means of quadratic constraints in the framework of Section 4.3.4 or, alternatively, without constraints in the framework of Section 4.3.5. Both alternative formulations are described in Appendix D.

One end of the beam structure is fixed, while at the other end a dead load of $\mathbf{F} = -10\mathbf{e}_1 - 10\mathbf{e}_3$ is applied in 30 equally spaced load steps. The beam stiffness parameters are given by $EA = 1 \times 10^4$, $GA = 5 \times 10^3$ and $EI = GI_p = 100/12$. The stopping criteria for Newton's method is set to $\|\mathbf{R}\| = 1 \times 10^{-10}$. Each beam segment is discretized with 3 finite elements of order $p = 3$.

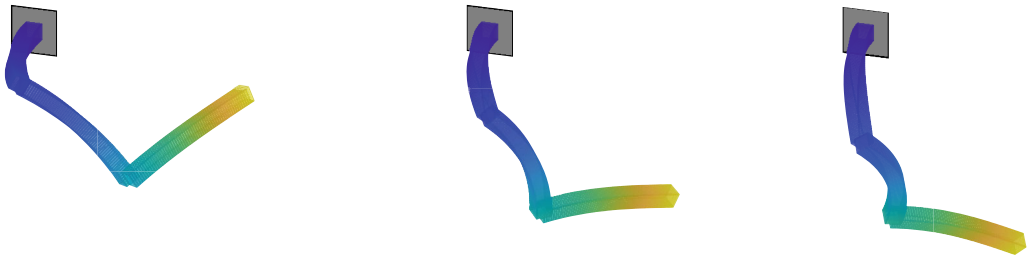

FIGURE 9 Configuration of the beam patches for different load levels. (A) Load level: $\frac{1}{3}\mathbf{F}$ – 10 load steps. (B) Load level: $\frac{2}{3}\mathbf{F}$ – 20 load steps. (C) Load level: $\mathbf{F}$ – 30 load steps.

In Figure 8B the components of the tip deflection are plotted over the load level. Both NURBS (NPS3) and Lagrange (LPS3) elements are used with a strong enforcement of the unit-length constraint. It can be seen that the results of the NURBS and Lagrange elements agree very well. In particular, no difference can be observed in Figure 8B. Furthermore, the results are in very good agreement with those in References 36,44,45.

In Figure 9 different configurations of the deformed beam structure corresponding to different load levels are shown.

6 | CONCLUSION

We have presented the geometrically exact beam model in terms of unit-quaternions along with a consistent spatial discretization. The proposed discretization conserves the unit-length constraint on the unit-quaternions along the beam. Correspondingly, the orthonormality of the director frame is ensured throughout the discrete beam model. This feature of the proposed discretization is ensured by applying a projection approach which coincides with the normalization of the approximated quaternion field. In this connection both Lagrange shape functions and NURBS shape functions have been employed. It was shown that the projection approach yields objective and path-independent beam finite elements that exhibit superior convergence properties. In particular, shape functions based on polynomial order p exhibit convergence rates of $\mathcal{O}(h^{2p})$. In addition to that, the projection approach was shown to improve the coarse mesh behavior.

Although the projection approach ensures the unit-length of the discrete quaternion field, the redundancy of the quaternion degrees of freedom still needed to be resolved. To this end, we applied two alternative procedures. The first one is based on the method of Lagrange multipliers for the explicit enforcement of the unit-length constraint. The constraints can be either enforced in weak form or in strong form at the control/nodal points. We prefer the strong imposition of the unit-length constraint since it makes possible the elimination of the constraint forces along with the introduction of rotational degrees of freedom. This procedure circumvents the treatment of saddle point systems and retains the advantageous approximation properties of the projection-based finite element formulation.

In future work we intend to extend the present approach to dynamic problems. It might also be of interest to discretize quaternions and displacements of the centerline with different approximation order. Previous work in this direction led to promising results in the context of a director formulation of the geometrically exact beam model.[36]

ACKNOWLEDGMENTS

The first author would like to express his gratitude to Professor Jose J.Muñoz for hosting him at his lab at the Universitat Politñnica de Catalunya, where a lot of the programming for this work took place. Support for his research stay was provided by the Research Travel Grant of the Karlsruhe House of Young Scientists (KYHS). This support is gratefully acknowledged. Open Access funding enabled and organized by Projekt DEAL.

DATA AVAILABILITY STATEMENT

The data that support the findings of this study are available from the corresponding author upon reasonable request.

ENDNOTES

*For simplicity, we content ourselves here with initially straight beams. The extension to initially curved beams is straightforward, see, for example, References 8 and 36.

†Note that we here assume a knot vector with unique entries in the interior leading to a C^{p-1} continuous basis.

ORCID

Peter Betsch https://orcid.org/0000-0002-0596-2503

REFERENCES

1. Reissner E. On one-dimensional finite-strain beam theory: The plane problem. *Z Angew Math Phys ZAMP*. 1972;23(5):795-804.
2. Simo JC. A finite strain beam formulation. The three-dimensional dynamic problem. Part I. *Comput Methods Appl Mech Eng*. 1985;49(1):55-70.
3. Antman SS. *Nonlinear Problems of Elasticity*. Springer-Verlag; 2005.
4. Holm DD, Schmah T, Stoica C. *Geometric Mechanics and Symmetry: From Finite to Infinite Dimensions*. Vol 12. Oxford University Press; 2009.
5. Howe R. Very basic Lie theory. *Am Math Mon*. 1983;90(9):600-623.
6. Sola J, Deray J, Atchuthan D. A micro Lie theory for state estimation in robotics. arXiv preprint, arXiv: 1812.01537 2018.
7. Stuelpnagel J. On the parametrization of the three-dimensional rotation group. *SIAM Review*. 1964;6(4):422-430.
8. Betsch P, Steinmann P. Frame-indifferent beam finite elements based upon the geometrically exact beam theory. *Int J Numer Methods Eng*. 2002;54(12):1775-1788.
9. Betsch P, Steinmann P. Constrained dynamics of geometrically exact beams. *Comput Mech*. 2003;31:49-59.
10. Romero I, Armero F. An objective finite element approximation of the kinematics of geometrically exact rods and its use in the formulation of an energy–momentum conserving scheme in dynamics. *Int J Numer Methods Eng*. 2002;54(12):1683-1716.
11. Romero I. The interpolation of rotations and its application to finite element models of geometrically exact rods. *Comput Mech*. 2004;34:121-133. doi:10.1007/s00466-004-0559-z
12. Ghosh S, Roy D. Consistent quaternion interpolation for objective finite element approximation of geometrically exact beam. *Comput Methods Appl Mech Eng*. 2008;198(3-4):555-571.
13. Bauchau O, Han S. Interpolation of rotation and motion. *Multibody Syst Dyn*. 2014;31:339-370.
14. Cottrell JA, Hughes TJR, Bazilevs Y. *Isogeometric Analysis - Toward Integration of CAD and FEA*. John Wiley and Sons, Ltd; 2009.
15. Hanson AJ. *Visualizing Quaternions*. Elsevier; 2005.
16. Dam E, Koch M, Lillholm M. *Quaternions, Interpolation and Animation*. Vol 2. Citeseer; 1998.
17. Cottanceau E, Thomas O, Véron P, Alochet M, Deligny R. A finite element/quaternion/asymptotic numerical method for the 3D simulation of flexible cables. *Finite Elem Anal Des*. 2018;139:14-34.
18. Dichmann D, Li Y, Maddocks J. Hamiltonian formulations and symmetries in rod mechanics. *Mathematical Approaches to Biomolecular Structure and Dynamics*. IMA Volumes in Mathematics and its Applications. Vol 82. Springer; 1996:71-113.
19. Sander O. Geodesic finite elements for Cosserat rods. *Int J Numer Methods Eng*. 2010;82(13):1645-1670. doi:10.1002/nme.2814
20. Crisfield MA, Jelenic G. Objectivity of strain measures in the geometrically exact three-dimensional beam theory and its finite-element implementation. *Proc R Soc A*. 1999;455:1125-1147.
21. Simo J, Vu-Quoc L. A three-dimensional finite-strain rod model. Part II: computational aspects. *Comput Methods Appl Mech Eng*. 1986;58:79-116.
22. Simo JC, Tarnow N, Doblare M. Non-linear dynamics of three-dimensional rods: Exact energy and momentum conserving algorithms. *Int J Numer Methods Eng*. 1995;38(9):1431-1473.
23. Cardona A, Géradin M. A beam finite element non-linear theory with finite rotations. *Int J Numer Meth Engng*. 1988;26:2403-2438.
24. Ibrahimbegović A. Finite element implementation of Reissner's geometrically nonlinear beam theory: three dimensional curved beam finite elements. *Comput Methods Appl Mech Eng*. 1995;122:10-26.
25. Sonneville V, Cardona A, Brüls O. Geometrically exact beam finite element formulated on the special Euclidean group SE(3). *Comput Methods Appl Mech Eng*. 2014;268:451-474. doi:10.1016/j.cma.2013.10.008
26. Harsch J, Sailer S, Eugster SR. A total Lagrangian, objective and intrinsically locking-free Petrov–Galerkin SE (3) Cosserat rod finite element formulation. *Int J Numer Methods Eng*. 2023;124(13):2965-2994.
27. Zupan E, Saje M, Zupan D. The quaternion-based three-dimensional beam theory. *Comput Methods Appl Mech Eng*. 2009;198(49-52):3944-3956.
28. Zupan E, Zupan D. On conservation of energy and kinematic compatibility in dynamics of nonlinear velocity-based three-dimensional beams. *Nonlinear Dyn*. 2019;95(2):1379-1394.
29. Weeger O, Wever U, Simeon B. Isogeometric analysis of nonlinear Euler–Bernoulli beam vibrations. *Nonlinear Dyn*. 2013;72:813-835.
30. Gawlik E, Leok M. Embedding-based interpolation on the special orthogonal group. *SIAM J Sci Comput*. 2018;40(2):A721-A746.
31. Grohs P, Hardering H, Sander O, Sprecher M. Projection-based finite elements for nonlinear function spaces. *SIAM J Numer Anal*. 2019;57(1):404-428. doi:10.1137/18M1176798
32. Müller A, Bischoff M. A consistent finite element formulation of the geometrically non-linear Reissner-Mindlin shell model. *Arch Comput Method E*. 2022; 29(5):3387-3434. doi:10.1007/s11831-021-09702-7

33. Leyendecker S, Betsch P, Steinmann P. The discrete null space method for the energy-consistent integration of constrained mechanical systems. Part III: Flexible multibody dynamics. *Multibody Syst Dyn*. 2008;19(1-2):45-72.
34. Betsch P, Siebert R. Rigid body dynamics in terms of quaternions: Hamiltonian formulation and conserving numerical integration. *Int J Numer Methods Eng*. 2009;79(4):444-473. doi:10.1002/nme.2586
35. Curtis ML. *Matrix groups*. Springer; 1984.
36. Harsch J, Capobianco G, Eugster SR. Finite element formulations for constrained spatial nonlinear beam theories. *Math Mech Solids*. 2021; 26(12):1838-1863.
37. Absil PA, Mahony R, Trumpf J. An extrinsic look at the Riemannian hessian. In: Nielsen F, Barbaresco F, eds. *Geometric Science of Information GSI*. Springer Berlin Heidelberg; 2013:361-368.
38. Piegl L, Tiller W. *The NURBS Book*. Springer-Verlag Berlin Heidelberg GmbH; 1997.
39. Betsch P. The discrete null space method for the energy consistent integration of constrained mechanical systems. Part I: Holonomic constraints. *Comput Method Appl M*. 2005;194(50-52):5159-5190.
40. Betsch P, Leyendecker S. The discrete null space method for the energy consistent integration of constrained mechanical systems. Part II: Multibody dynamics. *Int J Numer Methods Eng*. 2006;67(4):499-552.
41. Spurrier RA. Comment on "Singularity-free extraction of a quaternion from a direction-cosine matrix". *J Spacecr Rocket*. 1978;15(4):255.
42. Dornisch W, Klinkel S, Simeon B. Isogeometric Reissner-Mindlin shell analysis with exactly calculated director vectors. *Comput Methods Appl Mech Eng*. 2013;253:491-504.
43. Hughes T, Cottrell J, Bazilevs Y. Isogeometric analysis: CAD, finite elements, NURBS, exact geometry and mesh refinement. *Comput Methods Appl Mech Eng*. 2005;194(39):4135-4195.
44. Romero I. A comparison of finite elements for nonlinear beams: the absolute nodal coordinate and geometrically exact formulations. *Multibody Syst Dyn*. 2008;20(1):51-68.
45. Eugster SR, Hesch C, Betsch P, Glocker C. Director-based beam finite elements relying on the geometrically exact beam theory formulated in skew coordinates. *Int J Numer Methods Eng*. 2014;97(2):111-129.

How to cite this article: Wasmer P, Betsch P. A projection-based quaternion discretization of the geometrically exact beam model. *Int J Numer Methods Eng*. 2024;e7538. doi: 10.1002/nme.7538

APPENDIX A. STRAIN MEASURE FOR BENDING AND TWIST

We verify that strain measure (27) corresponds to the axial vector of the skew-symmetric matrix (26). Accordingly, one has to show that $\mathbf{K} = 2\mathbf{G}(\mathbb{q})\mathbb{q}_{,s}$ is the axial vector of matrix $2\mathbf{G}(\mathbb{q})\mathbf{G}(\mathbb{q}_{,s})^{\mathsf{T}}$. To see this, consider the identity

$$\mathbf{G}(\mathbb{q})\mathbb{q}_{,s} = -q_{0_{,s}}\mathbf{q} + q_0\mathbf{q}_{,s} - \mathbf{q}\times\mathbf{q}_{,s}. \tag{A1}$$

The skew-symmetric matrix associated with the above vector is given by

$$\begin{aligned}\mathbf{S} &= -q_{0_{,s}}\hat{\mathbf{q}} + q_0\hat{\mathbf{q}}_{,s} - \widehat{\mathbf{q}\times\mathbf{q}_{,s}} \\ &= -q_{0_{,s}}\hat{\mathbf{q}} + q_0\hat{\mathbf{q}}_{,s} - \left(\mathbf{q}_{,s}\otimes\mathbf{q} - \mathbf{q}\otimes\mathbf{q}_{,s}\right).\end{aligned} \tag{A2}$$

Since $\hat{\mathbf{a}}\hat{\mathbf{b}} = \mathbf{b}\otimes\mathbf{a} - (\mathbf{a}\cdot\mathbf{b})\mathbf{I}_3$ for any $\mathbf{a},\mathbf{b}\in\mathbb{R}^3$,

$$\mathbf{q}_{,s}\otimes\mathbf{q} = \hat{\mathbf{q}}\hat{\mathbf{q}}_{,s} + (\mathbf{q}_{,s}\cdot\mathbf{q})\mathbf{I}_3. \tag{A3}$$

Moreover, since $\mathbb{q}\in S^3$ implies $\mathbb{q}_{,s}\cdot\mathbb{q} = 0$ or $\mathbf{q}_{,s}\cdot\mathbf{q} = -q_{0_{,s}}q_0$, we eventually obtain

$$\mathbf{S} = -q_{0_{,s}}\hat{\mathbf{q}} + q_0\hat{\mathbf{q}}_{,s} + \mathbf{q}\otimes\mathbf{q}_{,s} - \hat{\mathbf{q}}\hat{\mathbf{q}}_{,s} + q_0q_{0_{,s}}\mathbf{I}_3. \tag{A4}$$

A direct calculation yields the result $\mathbf{G}(\mathbb{q})\mathbf{G}(\mathbb{q}_{,s})^{\mathsf{T}} = \mathbf{S}$.

APPENDIX B. APPLICATION OF EXTERNAL TORQUES

In the examples dealt with in Sections 5.1 and 5.2 an external torque $\overline{\mathbf{m}} \in \mathbb{R}^3$ is applied at one end of the beam. Since the collocation property holds at the end-points of both finite element formulations under consideration, the contribution to the weak form is given by

$$\begin{aligned} G^e_{\text{ext}} &= \delta \mathbb{q}_e \cdot 2\mathbf{E}(\mathbb{q}_e)^\top \overline{\mathbf{m}} \\ &= \delta \mathbb{p}_e \cdot \frac{1}{\|\mathbb{p}_e\|}(\mathbf{I}_4 - \mathbb{q}_e \otimes \mathbb{q}_e) 2\mathbf{E}(\mathbb{q}_e)^\top \overline{\mathbf{m}} \\ &= \delta \mathbb{p}_e \cdot \frac{2}{\|\mathbb{p}_e\|^2}\mathbf{E}(\mathbb{p}_e)^\top \overline{\mathbf{m}}, \end{aligned} \tag{B1}$$

where the quaternion normalization procedure has been accounted for. Furthermore, index e refers to the control/nodal point at the end of the beam. While in Section 5.1 the external torque $\overline{\mathbf{m}} = M\mathbf{e}_3$ can be directly inserted into the above formula, the external torque in Section 5.2 is a follower load defined by $\overline{\mathbf{m}} = \overline{m}^i \mathbf{d}^e_i = \mathbf{E}(\mathbb{q}_e)\mathbf{G}(\mathbb{q}_e)^\top \overline{m}^i \mathbf{e}_i$. Inserting this expression into the above formula yields

$$G^e_{\text{ext}} = \delta \mathbb{p}_e \cdot \frac{2}{\|\mathbb{p}_e\|^2}\mathbf{G}(\mathbb{p}_e)^\top \overline{m}^i \mathbf{e}_i. \tag{B2}$$

Here, the normalization procedure along with the properties summarized in (16) have been taken into account.

APPENDIX C. NUMERICAL PATH-INDEPENDENCE TEST

As mentioned in Section 5.3 we here show the results for other discretizations with 8, 16, and 32 elements and element order $p = 1, \dots, 3$. The number of elements is analogous to the results found in Reference 8, where only results for a first order discretization are shown. As we use NURBS basis functions we are able to conserve the geometry of the 1/8-circle exactly for the order $p = 2, 3$. For this purpose the initial control points of the NURBS formulation and their weights were computed with an algorithm from Chap. 7.5 in Reference 38 to define a section of a circle in combination with the refinement strategy for k-refinement in Chap. 5.5 in Reference 38 and for h-refinement in Reference 43 as mentioned in Section 5.

All values are evaluated for the same loads as in Table 3.

TABLE C1 Numerical path-independence test: tip displacement in 2-direction corresponding to specific load levels–additional results for different number of elements and linear elements ($p = 1$).

Tip displacement in 2-direction		
Lagrange elements (LPS1)		
8 el.	**16 el.**	**32 el.**
0	0	0
-8.9232×10^{-20}	-8.6515×10^{-20}	-8.844×10^{-20}
59.7206	59.8038	59.8262
38.5488	38.6585	38.6875
37.3891	37.4987	37.5269
-1.5671×10^{-11}	-1.6225×10^{-11}	-1.6362×10^{-11}
4.1576×10^{-22}	-4.9593×10^{-23}	1.2632×10^{-23}

TABLE C2 Numerical path-independence test: tip displacement in 2-direction corresponding to specific load levels–additional results for different number of elements and linear elements ($p = 1$).

Tip displacement in 2-direction		
NURBS elements (NPS1)		
8 el.	**16 el.**	**32 el.**
0	0	0
1.2277×10^{-14}	-1.1828×10^{-15}	-2.3202×10^{-14}
59.7132	59.8029	59.8261
38.5469	38.6584	38.6875
37.3916	37.4491	37.5270
-1.5783×10^{-11}	-1.6246×10^{-11}	-1.6369×10^{-11}
-1.1852×10^{-15}	9.2804×10^{-16}	-7.8410×10^{-16}

TABLE C3 Numerical path-independence test: tip displacement in 2-direction corresponding to specific load levels–additional results for different number of elements and quadratic elements ($p = 2$).

Tip displacement in 2-direction		
Lagrange elements (LPS2)		
8 el.	**16 el.**	**32 el.**
0	0	0
1.8588×10^{-17}	6.4369×10^{-18}	9.3133×10^{-21}
58.6129	59.7042	59.8232
37.7556	38.5692	38.6869
35.7855	37.3584	37.5233
-1.1916×10^{-11}	-1.6153×10^{-11}	-1.6386×10^{-11}
-7.4184×10^{-20}	-1.002×10^{-21}	8.9024×10^{-22}

TABLE C4 Numerical path-independence test: tip displacement in 2-direction corresponding to specific load levels–additional results for different number of elements and quadratic elements ($p = 2$).

Tip displacement in 2-direction		
NURBS elements (NPS2)		
8 el.	**16 el.**	**32 el.**
0	0	0
-4.9258×10^{-14}	-1.1828×10^{-15}	-2.3202×10^{-14}
57.6927	59.5842	59.8542
37.1466	38.4948	38.7195
35.1708	37.3045	37.5619
-8.6269×10^{-12}	-1.5806×10^{-11}	-1.6403×10^{-11}
5.0916×10^{-14}	6.6981×10^{-15}	-1.4206×10^{-14}

TABLE C5 Numerical path-independence test: tip displacement in 2-direction corresponding to specific load levels–additional results for different number of elements and cubic elements ($p = 3$).

Tip displacement in 2-direction		
Lagrange elements (LPS3)		
8 el.	**16 el.**	**32 el.**
0	0	0
-2.7663×10^{16}	5.9239×10^{-20}	-1.275×10^{-19}
59.8085	59.8332	59.8338
38.6732	38.6969	38.6974
37.5207	37.5361	37.5364
-1.6403×10^{-11}	-1.6408×10^{-11}	-1.6407×10^{-11}
-1.9518×10^{-21}	-2.0485×10^{-23}	-2.2070×10^{-12}

TABLE C6 Numerical path-independence test: tip displacement in 2-direction corresponding to specific load levels–additional results for different number of elements and cubic elements ($p = 3$).

Tip displacement in 2-direction		
NURBS elements (NPS3)		
8 el.	**16 el.**	**32 el.**
0	0	0
-2.8256×10^{-14}	-1.0551×10^{-14}	-8.5072×10^{-15}
59.7312	59.8724	59.8754
38.6098	38.7347	38.7374
37.5061	37.5795	37.5809
-1.6504×10^{-11}	-1.6453×10^{-11}	-1.6448×10^{-11}
4.3234×10^{-16}	2.6724×10^{-15}	-2.5779×10^{-15}

APPENDIX D. RIGID INTERSECTION BETWEEN TWO BEAMS

In this Appendix, we address the rigid connection of two beams as required in the numerical example in Section 5.4. In particular, we consider a rigid intersection between the end-points of two beams (Figure D1). Accordingly, the two end-points, say A and B, experience the same rotation $\mathbb{r} \in S^3$ with respect to some previous cross-sectional orientations $\mathbb{q}_A^0 \in S^3$ and $\mathbb{q}_B^0 \in S^3$. That is, the new cross-sectional orientations are given by $\mathbb{p}_A = \mathbb{r} \circ \mathbb{q}_A^0$ and $\mathbb{p}_B = \mathbb{r} \circ \mathbb{q}_B^0$. These two equations can be rewritten as $\mathbb{r} = \mathbb{p}_A \circ \overline{\mathbb{q}}_A^0$ and $\mathbb{r} = \mathbb{p}_B \circ \overline{\mathbb{q}}_B^0$, respectively. Since $\mathbb{r} \circ \overline{\mathbb{r}} = (1, 0)$, we obtain

$$\mathbb{p}_A \circ \overline{\mathbb{q}}_A^0 \circ \mathbb{q}_B^0 \circ \overline{\mathbb{p}}_B = (1, 0). \tag{D1}$$

We take the vector part of the above condition to obtain three equations of constraint to impose the rigid intersection between the two beams. Three more conditions arise from the additional constraint $\boldsymbol{\varphi}_A - \boldsymbol{\varphi}_B = 0$. Accordingly, the rigid coupling of two beams can be realized by appending a total of six algebraic constraints to the beam formulation in Section 4.3.4.

Alternatively, algebraic constraints can be circumvented by applying the discrete null space method outlined in Section 4.3.5. Accordingly, starting with the constrained formulation in Section 4.3.4, the quantities $(\boldsymbol{\varphi}_B, \mathbb{p}_B)$ and $(\delta\boldsymbol{\varphi}_B, \delta\mathbb{p}_B)$ related to control/nodal point B can be expressed in terms of the corresponding quantities in point A via

$$\boldsymbol{\varphi}_B = \boldsymbol{\varphi}_A, \tag{D2}$$

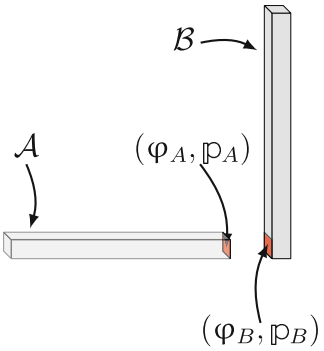

FIGURE D1 Sketch of two rigidly connected beams $\mathcal{A}$ and $\mathcal{B}$.

$$\mathbb{p}_B = \mathbb{p}_A \circ \overline{\mathbb{q}}^0_A \circ \mathbb{q}^0_B, \tag{D3}$$

and

$$\delta\boldsymbol{\varphi}_B = \delta\boldsymbol{\varphi}_A, \tag{D4}$$

$$\delta\mathbb{p}_B = \delta\mathbb{p}_A \circ \overline{\mathbb{q}}^0_A \circ \mathbb{q}^0_B. \tag{D5}$$

A further size-reduction of the algebraic system to be solved can be achieved by applying the procedure described in Section 4.3.5.